

### [<sup>3</sup>H]Thymidine Incorporation Assay

Cortical embryonic NPCs were seeded in 96-well plates ( $1 \times 10^4$  cells/well) in 100  $\mu$ L of medium and cultured for 24 h at 37°C with b-FGF (5 ng/mL). Vehicle or peptide (PACAP38, 0–100 nM; maxadilan, 0–10 nM; or M65, 10 nM) was then added; after 1 h, 1  $\mu$ Ci/well [<sup>3</sup>H]thymidine was also added. After a 7-h incubation, the cells were washed extensively with medium, and [<sup>3</sup>H]thymidine incorporation was measured using a  $\beta$ -counter.

For the CM proliferation assay, embryonic cortical NPCs were seeded in 96-well plates ( $1 \times 10^4$  cells/well) in 100  $\mu$ L of medium and cultured for 24 h at 37°C. Medium was then replaced with NPC conditioned medium or control medium. [<sup>3</sup>H]thymidine incorporation and measurement were performed as described above.

To assess PAC1 signaling, cortical embryonic NPCs were seeded in 96-well plates ( $10^4$  cells/well) in 100  $\mu$ L of medium and cultured for 24 h at 37°C. Cells were pre-incubated for an additional 1 h with vehicle and signal transduction inhibitors (H89, 10  $\mu$ M 2-APB, 20  $\mu$ M; chelerythrine, 50  $\mu$ M), and then maxadilan (10 nM) was added. [<sup>3</sup>H]thymidine incorporation was measured as described above.

### Intracellular ATP Assays

It has been previously reported that intracellular ATP levels correlate with cell number (Crouch et al., 1993). Embryonic cortical NPCs were seeded in 48-well plates ( $4.5 \times 10^4$  cells/well) in 400  $\mu$ L of medium and cultured for 24 h at 37°C with b-FGF (5 ng/mL). After 24 h, each peptide (PACAP38, 0–100 nM; maxadilan, 0–10 nM; PACAP(6–38), 10 nM) was added to these NPC cultures. After a 6 or 24-h incubation with the peptides, intracellular ATP levels were measured using the CellTiter-Glo Luminescent Cell Viability Assay kit (Promega, Madison, WI) according to the manufacturer's instructions.

### Radioimmunoassay for PACAP38

PACAP38 concentration was measured in conditioned medium derived from NPCs using a radioimmunoassay (RIA). Cell-free conditioned medium (100  $\mu$ L) and conditioned medium derived from NPCs (100  $\mu$ L) were incubated with polyclonal anti-PACAP38, which was rehydrated in RIA buffer (Phoenix Pharmaceuticals, Belmont, CA) for 24 h at 4°C. These reactions were incubated with <sup>125</sup>I-PACAP(31–38) (50 cpm/ $\mu$ L) for an additional 24 h at 4°C. Second antibody reaction/separation and detection of <sup>125</sup>I in the pellets were performed in a scintillation well gamma counter according to the instrument manufacturer's instructions (Phoenix Pharmaceuticals, Belmont, CA).

GLIA DOI 10.1002/glia

### Intracellular cAMP Measurement

Cortical embryonic NPCs were seeded in 96-well plates and treated with PACAP38 (100 nM) or maxadilan (10 nM) for 24 h. cAMP levels were assayed by the cAMP-Screen™ System (Applied Biosystems).

### Intracellular Calcium Imaging

Cortical embryonic NPCs were seeded in 96-well plates and cultured for 24 h as described above for the intracellular cAMP measurement. The intracellular concentration of free calcium ([Ca<sup>2+</sup>]<sub>i</sub>) in cultured NPCs was monitored using the Calcium Kit-Fluo 3 (Dojindo Laboratories, Kumamoto, Japan) according to the manufacturer's instructions. For a negative control, cells were pre-incubated for an additional 1 h with BAPTA-AM (100  $\mu$ M), and then PACAP38 (100 nM) or maxadilan (10 nM) was added.

## RESULTS

### Expression of PAC1 and PACAP in Embryonic Cortical NPCs In Vivo and In Vitro

To generate a highly purified population of embryonic cortical NPCs, we prepared a secondary culture of NPCs (Li et al., 2001; Nakashima et al., 1999). Most of these cells were positive for nestin, a specific marker for NPCs in developmental brain, but less than 0.5% were immunoreactive for  $\beta$  III tubulin and GFAP. Gal C positive cells were not found (data not shown).

We used RT-PCR and immunohistochemical methods to investigate PAC1 and PACAP expression in cultured mouse embryonic cortical NPCs. RT-PCR detected both PAC1 and PACAP mRNAs in the NPCs and mouse telencephalon at embryonic day 14.5 (Fig. 1A). Other PACAP receptors, VPAC1 and VPAC2, mRNAs were expressed at a much lower level [(0.01  $\pm$  1.7)% and (0.11  $\pm$  2.3)% (mean  $\pm$  S.E.M.), respectively] than PAC1 mRNA (33.1  $\pm$  0.23)% (Fig. 1A). In addition, the mRNA for another PAC1 ligand, VIP, was not detected in embryonic cortical NPCs (Fig. 1A). In immunohistochemistry experiments, PACAP protein was expressed in nestin-immunoreactive NPCs, and most nestin-immunoreactive NPCs expressing PAC1 colocalized with PACAP in the VZ and SVZ (Fig. 1B). We also detected PACAP and PAC1 in nestin-immunoreactive cultured embryonic cortical NPCs. Over 99.8% of the PAC1-expressing cells co-expressed PACAP (Fig. 1C).

### Activation of PAC1 Signaling Induces Embryonic Cortical NPC Proliferation in the Presence of b-FGF in an Autocrine Manner

We performed a [<sup>3</sup>H]thymidine incorporation assay and an ATP assay, which measures intracellular ATP

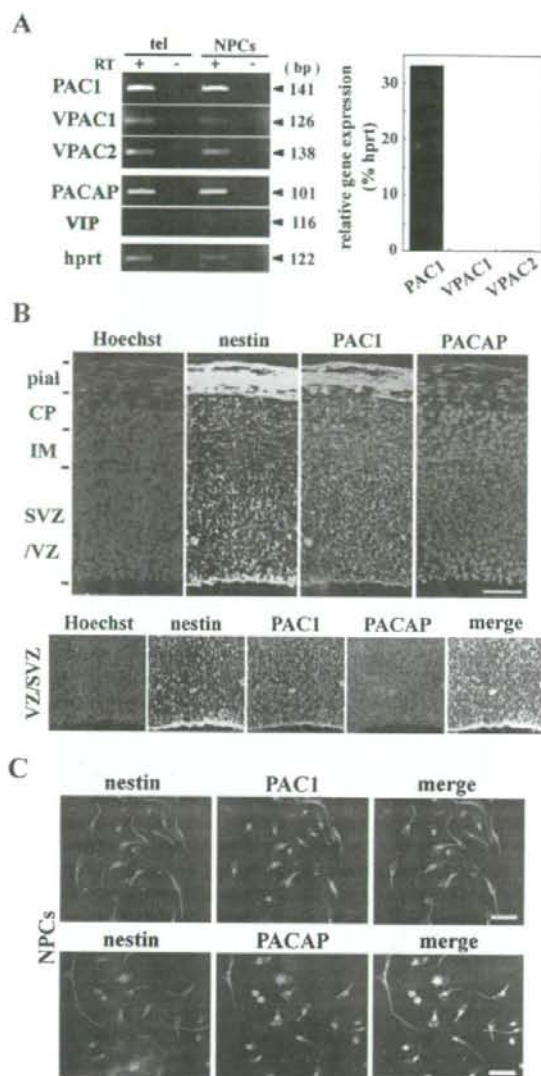


Fig. 1. NPCs express the PACAP receptors PAC1, VPAC1 and VPAC2, and their ligand, PACAP. **A**: RT-PCR was performed as described in Material and Methods. PCR products corresponding to these receptor and ligand genes were loaded onto a 3% agarose gel, as indicated at the left. The size of the PCR products is indicated on the right. Quantitative analysis of mRNA transcripts for PACAP receptors in NPCs by SYBER green-based PCR 7700 system. Data represents expression level of individual PACAP receptors relative to the expression level of hprt. **B,C**: PACAP is an autocrine factor of NPCs. PAC1 and PACAP protein expression was determined by immunofluorescence in vivo (**B**) and in vitro (**C**). Nestin-immunoreactive cells (cyan) in E14.5 mouse embryonic telencephalon also expressed PAC1 (green) and PACAP (red). The lower panels are high magnifications of the upper panels (**B**). Cell nuclei were counterstained with Hoechst 33258 (blue, **B**). Almost all nestin-immunoreactive NPCs (red, **C**) expressed PAC1 (green, top panel in **C**) and PACAP (green, lower panel in **C**). Cell nuclei were counterstained with Hoechst 33258 (blue, **C**). Scale bars: (**B**, **C**) 50  $\mu$ m.

levels and hence indicates the viable cell number, to determine whether PAC1 signaling promotes NPC proliferation. A 6-h incubation neither with PACAP38 (0–100 nM), the natural ligand for PAC1, nor with maxadilan (0–1 nM), a specific agonist for PAC1, induced DNA synthesis in the absence of b-FGF (Fig. 2A). In contrast, both reagents increased [ $^3$ H]thymidine incorporation in a dose-dependent manner in the presence of b-FGF without altering the viable cell number as assessed by the ATP assay (Figs. 2A,B). After incubation for 24 h, maxadilan increased intracellular ATP levels in the presence of b-FGF, and this increase was completely inhibited by the PAC1-specific antagonist, PACAP(6–38) (Fig. 2C). The PAC1 ligand, VIP, also increased [ $^3$ H]thymidine incorporation in NPCs (Fig. 2D) after incubation for 6 h. However, the DNA synthesis-promoting activity of VIP was lower than that of PACAP38 or maxadilan, and was inhibited by PACAP(6–38) (data not shown). These results indicate that activation of PAC1 promotes DNA synthesis in 6 h followed by NPC proliferation in 24 h in cultures supplemented with b-FGF.

To investigate whether PACAP secreted from embryonic cortical NPCs induces DNA synthesis in the presence of b-FGF, we analyzed [ $^3$ H]thymidine incorporation in NPCs cultured with conditioned medium derived from embryonic cortical NPCs supplemented with b-FGF. After 7 h, [ $^3$ H]thymidine incorporation increased by 140% relative to NPCs cultured with NPC-free media, and this activity was inhibited by another PAC1-specific antagonist, M65 (Fig. 3). Similar inhibition was observed when PACAP(6–38) was used (data not shown). We also performed a radioimmunoassay to detect PACAP38 in the conditioned medium derived from NPCs. The PACAP concentration was substantially higher in conditioned medium derived from NPCs ( $284 \pm 2.3$  pg/mL, Mean  $\pm$  SEM) than in NPC-free medium ( $0.072 \pm 0.25$  pg/mL, Mean  $\pm$  SEM).

#### PLC/IP<sub>3</sub> Signaling Pathway are Activated by Maxadilan Via PAC1 Splice Variants in Embryonic Cortical NPCs

To determine which splice variant (or variants) was expressed in our embryonic cortical NPCs, we performed RT-PCR using splice variant-specific primer pairs. We detected four PAC1 variants (Fig. 4).

To determine whether PAC1 couples to the cAMP pathway, we measured intracellular cAMP concentration in NPCs after treatment with PACAP38 or maxadilan. Both reagents elicited a 3.5–4-fold increase in intracellular cAMP concentration (Fig. 5A). We used the Fluo-3 ratio method to determine the effects of PAC1 activation on calcium signaling. The intracellular calcium level ( $[Ca^{2+}]_i$ ) increased rapidly in NPCs following treatment with PACAP38 or maxadilan (Fig. 5B). This activity was inhibited by BAPTA-AM, which was an intracellular  $Ca^{2+}$ -chelator (Fig. 5B). We used pathway-specific in-

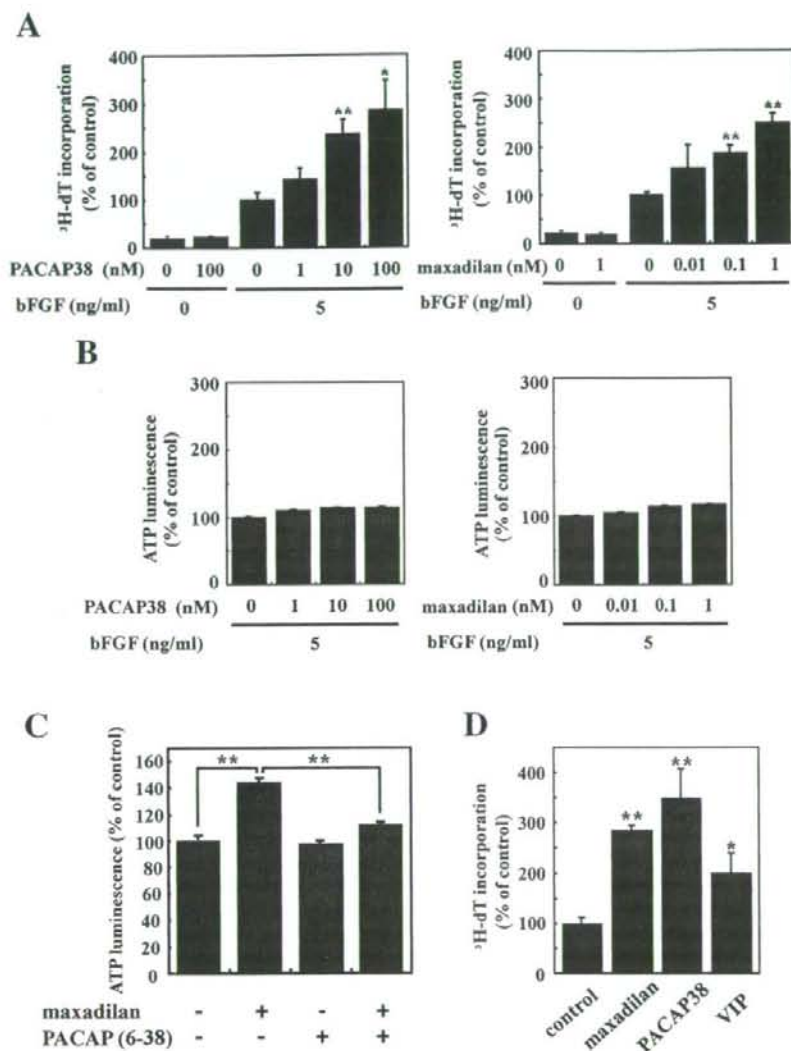


Fig. 2. PAC1 signaling promotes NPC growth in the presence of b-FGF. **A,B:** PACAP38 and maxadilan promote DNA synthesis and cell growth of NPCs in a dose-dependent manner in the presence of b-FGF. NPCs were cultured with PACAP38 (0–100 nM) (left) or maxadilan (0–1 nM) (right) in the presence or absence of b-FGF (5 ng/mL) for 7 h, and then [<sup>3</sup>H]thymidine was added during the last 6 h of culture (**A**). NPCs were cultured with PACAP38 (left) or maxadilan (right) in the presence of b-FGF (5 ng/mL) for 6 h, and then the growth rate was examined by an ATP luminescence assay (**B**). **C:** The PAC1-specific agonist, maxadilan, promotes NPC growth; blockade of PAC1 with the PAC1-specific antagonist, PACAP (6–38), completely cancels this growth-promoting activity. NPCs were incubated with or without maxadilan (1 nM) for 24 h. Maxadilan-induced cell growth was inhibited by co-incubation with PACAP (6–38) (10 nM). **D:** NPCs were cultured with or without PACAP38 (100 nM), maxadilan (10 nM) or VIP (1  $\mu$ M) in the presence of b-FGF for 7 h, and then [<sup>3</sup>H]thymidine was added during the last 6 h of culture. Bars represent mean  $\pm$  SD ( $n = 4$ ). Significant differences from control (without agonist or antagonist) are indicated by asterisks (\* $P < 0.05$ ; \*\* $P < 0.01$ , ANOVA).

inhibitors for protein kinase A (PKA) or inositol 1,4,5-trisphosphate (IP<sub>3</sub>)/C kinase (PKC) to determine which signaling pathway mediates PAC1 activity during embryonic cortical NPC proliferation. H89, which inhibits cAMP-dependent PKA, did not inhibit the maxadilan-induced increase in [<sup>3</sup>H]thymidine incorporation; however, 2-APB, which inhibits the IP<sub>3</sub> receptor, had a strong inhibitory effect (Fig. 5C). In addition, chelerythrin, which inhibits PKC, did not inhibit the effect of maxadilan. Taken together, these results indicate that NPC proliferation involved the PLC/IP<sub>3</sub>-dependent signaling pathway and a downstream Ca<sup>2+</sup>-dependent pathway.

#### PAC1 Activation Induces NPC Proliferation and Morphological Changes in Embryonic Cortical NPCs

Upon maxadilan stimulation for 48 h, we observed a morphological change, which was an elongation of cell processes with stellate and astrocyte-like morphology, in nestin-immunoreactive NPCs (Fig. 6A). To determine the relationship between NPC proliferation and the morphological changes seen by PAC1 signaling, we identified nestin-immunoreactive NPCs in the mitotic phase with a BrdU incorporation assay. Immediately after 10 min of

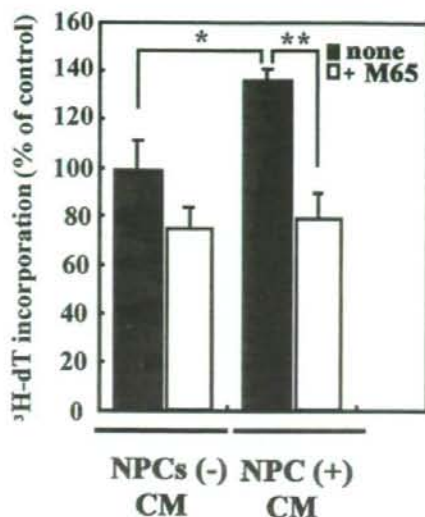


Fig. 3. The activation of PAC1-induced NPC proliferation in autocrine system. NPCs were cultured for 24 h, and the conditioned medium (CM) was collected. The CM or control cell-free media was added to freshly prepared NPC cultures and incubated for 7 h. [<sup>3</sup>H]thymidine was added during the last 6 h, and incorporation was later measured. DNA synthesis-promoting activity in CM was observed and this activity was inhibited by the PAC1-selective antagonist, M65 (10 nM). Bars represent mean  $\pm$  SD ( $n = 4$ ). Significant differences from the control are indicated by asterisks (\* $P < 0.05$ , \*\* $P < 0.01$ ; ANOVA).

exposure to BrdU, the unincorporated BrdU was washed off the NPCs and maxadilan (10 nM) was added in BrdU-free and b-FGF contained medium. After 24 h, maxadilan increased the number of BrdU/nestin immunoreactive NPCs with long cell processes compared with non-treated NPCs (Fig. 6B). Next, we addressed the differentiation of BrdU immunoreactive NPCs to neurons, astrocytes, or oligodendrocytes. We observed a gradual increase of BrdU immunoreactive NPCs by the 24-h treatment of maxadilan during 7 days, compared with non-treated NPCs. The treatment of maxadilan did not increase the number of  $\beta$  III tubulin immunoreactive neurons, whereas maxadilan induced marked increase of GFAP immunoreactive astrocytes. Moreover, we observed the significant increase in the percentage of BrdU/GFAP double immunoreactive astrocytes, compared with that of non-treated NPCs at day 7 (Figs. 6B–E). These data suggested that PAC1 signaling regulates the proliferation of glial progenitor cells to generate astrocytes in E14.5 NPCs.

## DISCUSSION

The PACAP/PAC1 system plays an important role in regulating differentiation of embryonic NPCs at E12–17 (Lee et al., 2001; Lelievre et al., 2002; Lu and DiCiccio-Bloom, 1997; Lu et al., 1998; Suh et al., 2001). In our results, the PACAP/PAC1 autocrine system potentiated

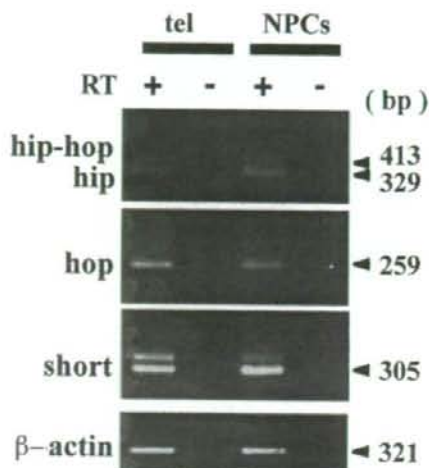


Fig. 4. NPCs express all PAC1 isoforms. RT-PCR was performed as described in Material and Methods. RT-PCR of E14.5 mouse embryonic telencephalon (tel) was used for comparison. The PCR products corresponding to the PAC1 isoforms were loaded onto a 3% agarose gel, as indicated at the left. The size of the PCR products is indicated on the right.

growth factor-promoted proliferation of E14.5 mouse cortical NPCs. Moreover, we found that the activation of PAC1 initiated morphological changes, which were cell process elongation of typical astrocytes in embryonic cortical NPCs. In the BrdU incorporation assay, most of BrdU positive NPCs differentiated to astrocytes. We suggest dual aspects of PAC1 signaling in the regulation of not only differentiation but also proliferation of NPCs at E14.5 via PLC/IP<sub>3</sub> signaling pathways through PAC1 variants in NPCs committed to an astrocytic lineage.

We found that the PACAP/PAC1 system potentiated growth factor-induced proliferation of E14.5 mouse cortical NPCs in an autocrine manner. Many trophic factor-generated microenvironments control NPC proliferation or differentiation. In particular, growth factors such as b-FGF, EGF, and TGF $\alpha$  promote NPC proliferation in the embryonic and postnatal brain (Gritti et al., 1996; Kilpatrick and Bartlett, 1993; Richards et al., 1992; Vescovi et al., 1999). Although these growth factors are soluble and thus diffuse widely in the CNS, their regulation during development has not been fully understood. In our results, immunoreactivity for PACAP and PAC1 in VZ/SVZ as well as the detection of PACAP38 in conditioned medium derived from NPCs supported the evidence of a PACAP/PAC1 autocrine loop in embryonic NPCs. Several molecules function in an autocrine manner in embryonic NPCs. BMPs and noggin are autocrine factors that regulate NPC proliferation and differentiation (Mabie et al., 1999; Nadarajah et al., 2002; Panchision et al., 2001; Sauvageot and Stiles, 2002). In adult brain, Cystatin C, IGF-I and stem cell-derived stem/progenitor cell-supporting factor have been charac-

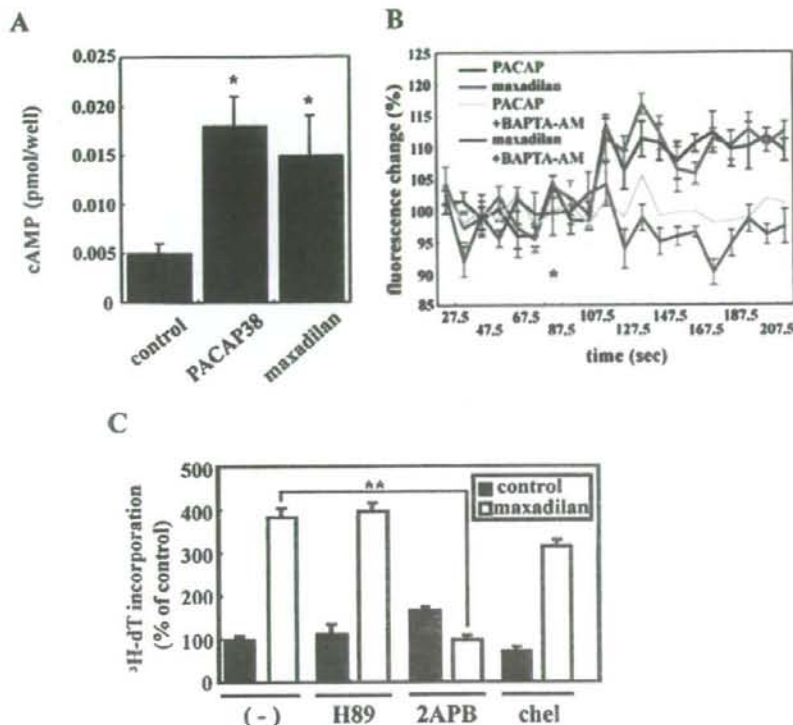


Fig. 5. PACAP promotes DNA synthesis in NPCs via PKC and IP<sub>3</sub>, but the PAC1-selective agonist, maxadilan, promotes the activity via IP<sub>3</sub> only. **A**: The activation of PAC1 increases intracellular cAMP level in NPCs. The intracellular cAMP content in NPCs was measured after treatment with PACAP38 (100 nM) or maxadilan (10 nM) for 15 min by ELISA system. **B**: The activation of PAC1 increases intracellular calcium level ( $[Ca^{2+}]_i$ ) in NPCs. The ratio of  $[Ca^{2+}]_i$  was analyzed by Fluo-3 AM imaging at the steady state and after the treatment\* of PACAP38 (100 nM) or maxadilan (10 nM). **C**: NPCs were incubated with 10  $\mu$ M H89, 2.5  $\mu$ M 2-APB or 100 nM chelerythrine in the presence of 5 ng/mL b-FGF for 1 h before the addition of 100 nM PACAP38 or 10 nM maxadilan. [<sup>3</sup>H]thymidine was added during the last 6 h of culture. Data represent mean values  $\pm$  SD ( $n = 4$ ). Significant differences from the control are indicated by asterisks (\* $P < 0.05$ , \*\* $P < 0.01$ ; ANOVA).

terized as autocrine/paracrine growth-supporting factors for adult NPC proliferation, which is promoted by b-FGF/EGF (Toda et al., 2003). These factors are required to maintain multipotent adult NPC proliferation (Toda et al., 2003). These autocrine systems, including the PACAP/PAC1 system, are considered to play an important role in restricting or amplifying growth factor-mediated signals and in controlling NPC proliferation and differentiation.

At an early developmental stage (E12–14) during which the mouse cortex undergoes neurogenesis, the PACAP/PAC1 system promotes neuronal differentiation of cortical NPCs (Dicicco-Bloom et al., 1998; Lee et al., 2001; Lu and DiCicco-Bloom, 1997; Suh et al., 2001). In contrast, cortical NPCs derived from a late stage (E17) promote astrocyte differentiation via PAC1 (Vallejo and Vallejo, 2002). Furthermore, at the postnatal stage, when oligogenesis occurs, PAC1 signaling regulates both the growth and differentiation of oligodendrocyte progenitor cells (Lee et al., 2001). Thus the PACAP/PAC1 system plays multiple roles in the different cell lineages during development, and this fact suggests that it may function via several signaling pathways. Recent studies have shown that Gs- or Gq-mediated intracellular signal via PAC1 splice variants induced a specific biological activity, differentiation or proliferation, in cortical pro-

genitor cells (Bresson-Bepoldin et al., 1998; Jaworski and Proctor, 2000; Lu et al., 1998; Zhou et al., 2000a,b). Our RT-PCR experiment showed that PAC1 splice variants were expressed in mouse embryonic cortical NPCs at E14.5. Moreover, we detected intracellular cAMP accumulation and  $[Ca^{2+}]_i$  increase via PAC1 activation in NPCs (Figs. 5A,B). These results suggested that the activation of PAC1 stimulated both Gs-mediated AC/PKA and Gq-mediated PLC/IP<sub>3</sub> signaling pathways in embryonic cortical NPCs at E14.5 via PAC1 variants. Although many studies have reported that AC/PKA signal induced NPC differentiation into neuron or glial cells via PAC1 (Zhou et al., 2001), the effects of PLC/IP<sub>3</sub> signal in NPC lineage is unknown. We found that IP<sub>3</sub> inhibitor curtailed PAC1-mediated NPC proliferation (Fig. 5C), suggesting that Gq-mediated PLC/IP<sub>3</sub>, not Gs-mediated AC/PKA, signaling pathway modulated NPC proliferation via the PAC1 variant which might give rise to different signaling pathways for NPC differentiation and proliferation.

Cortical NPCs at E14.5 may have heterogeneous subpopulations. Some of these are multipotent and others are committed to neuronal or glial progenitors which generate neurons or astrocytes (Sauvageot and Stiles, 2002). As indicated by our morphological study and BrdU labeling, PAC1 signaling potentiated the pro-

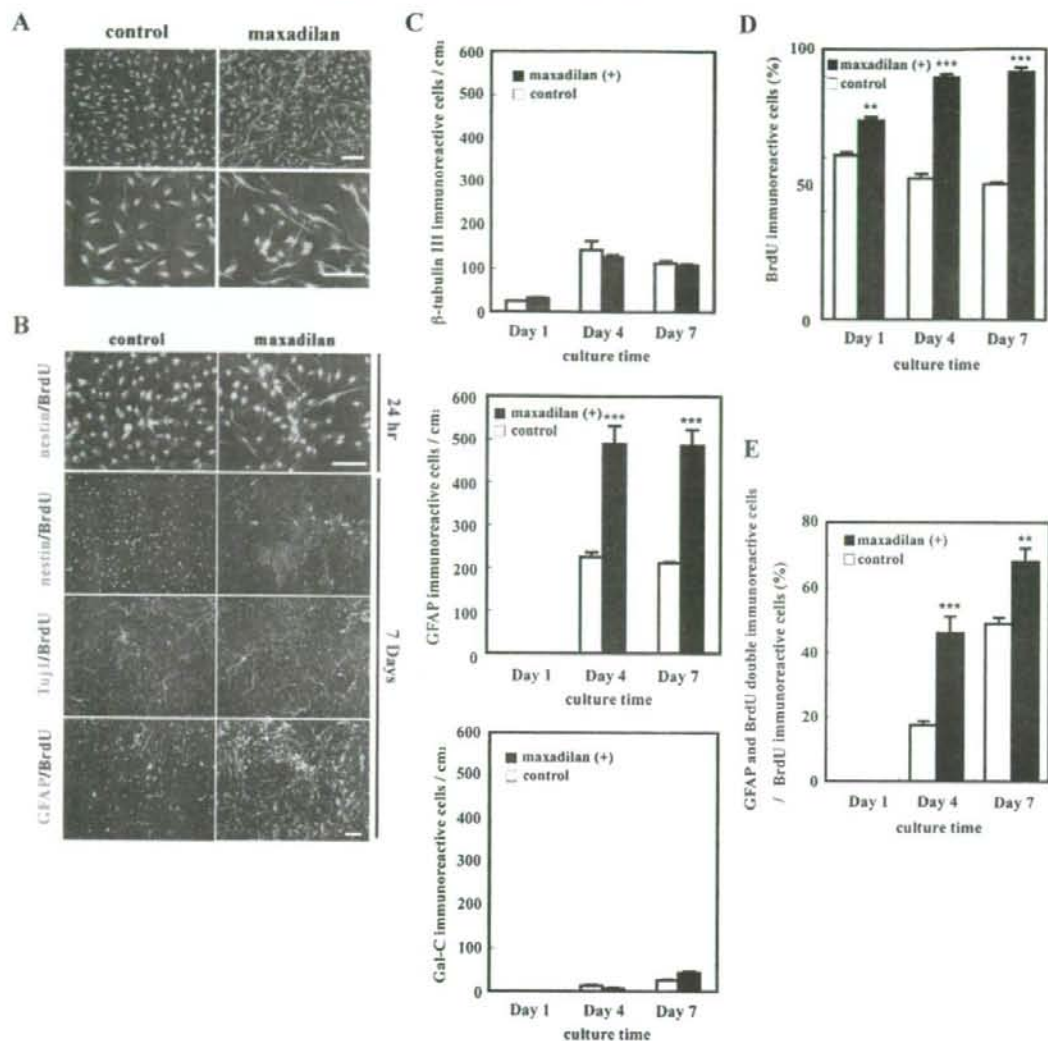


Fig. 6. PAC1 signaling promotes the proliferation of embryonic cortical NPCs committed to astrocytes. **A:** After maxadilan treatment for 24 h, cells were fixed and stained for nestin (green), Hoechst (blue) and BrdU (red). **B:** After maxadilan treatment for 7 days, cells were fixed and stained for nestin (green),  $\beta$  III tubulin (b III tub) (green), GFAP (green), Hoechst (blue) and BrdU (red). **C:** Quantitative analysis of differentiation of embryonic cortical NPCs treated or non-treated with maxadilan for 7 days. **D:** Proliferation of embryonic cortical NPCs treated or non-treated with maxadilan assessed by BrdU incorporation assay. **E:** Time course of astrogenesis from BrdU immunoreactive embryonic cortical NPCs treated or non-treated with maxadilan. Total cellular counts were obtained as described in Materials and Methods. Data represent mean values  $\pm$  SD ( $n = 4$ ). Significant differences from the control are indicated by asterisks (\* $P < 0.05$ , \*\* $P < 0.01$ , \*\*\* $P < 0.001$ ; ANOVA). Scale bars: (A, B) 50  $\mu$ m.

ated or non-treated with maxadilan assessed by BrdU incorporation assay. **E:** Time course of astrogenesis from BrdU immunoreactive embryonic cortical NPCs treated or non-treated with maxadilan. Total cellular counts were obtained as described in Materials and Methods. Data represent mean values  $\pm$  SD ( $n = 4$ ). Significant differences from the control are indicated by asterisks (\* $P < 0.05$ , \*\* $P < 0.01$ , \*\*\* $P < 0.001$ ; ANOVA). Scale bars: (A, B) 50  $\mu$ m.

liferation of NPCs with longer cell processes manifesting astrocyte-like shapes. Moreover, most BrdU immunoreactive NPCs were differentiated into GFAP immunoreactive astrocytes via PAC1. One of the autocrine factor families, BMPs, are reported to promote astrocytic differentiation and to change the proliferative activities of cortical NPCs in the different developmental stages (Gross

et al., 1996; Mabie et al., 1999). Our data may reflect a dual role for the PACAP/PAC1 system; potentiating glial progenitor cell proliferation and subsequent astrogenesis as well as astrocytic differentiation in NPCs similar to BMPs. The PACAP/PAC1 autocrine system is critical for the regulation of NPC and glial lineage, depending on the stage of brain development.

## ACKNOWLEDGMENTS

We thank Dr. Richard G. Titus for providing maxadilan and M65. We thank Mr. Ayukawa K. and Mrs. Hara Y. for the early work contribution and excellent technical help.

## REFERENCES

- Altman J, Bayer SA. 1990a. Horizontal compartmentation in the germinal matrices and intermediate zone of the embryonic rat cerebral cortex. *Exp Neurol* 107:36-47.
- Altman J, Bayer SA. 1990b. Vertical compartmentation and cellular transformations in the germinal matrices of the embryonic rat cerebral cortex. *Exp Neurol* 107:23-35.
- Arimura A. 1998. Perspectives on pituitary adenylate cyclase activating polypeptide (PACAP) in the neuroendocrine, endocrine, and nervous systems. *Jpn J Physiol* 48:301-331.
- Basille M, Gonzalez BJ, Desruets L, Demas M, Fournier A, Vaudry H. 1995. Pituitary adenylate cyclase-activating polypeptide (PACAP) stimulates adenylyl cyclase and phospholipase C activity in rat cerebellar neuroblasts. *J Neurochem* 65:1318-1324.
- Basille M, Gonzalez BJ, Leroux P, Jeandel L, Fournier A, Vaudry H. 1993. Localization and characterization of PACAP receptors in the rat cerebellum during development: Evidence for a stimulatory effect of PACAP on immature cerebellar granule cells. *Neuroscience* 57:329-338.
- Bluet-Pajot MT, Epelbaum J, Gourdji D, Hammond C, Kordon C. 1998. Hypothalamic and hypophysial regulation of growth hormone secretion. *Cell Mol Neurobiol* 18:101-123.
- Bresson-Bepoldin L, Jacquot MC, Schlegel W, Rawlings SR. 1998. Multiple splice variants of the pituitary adenylate cyclase-activating polypeptide type 1 receptor detected by RT-PCR in single rat pituitary cells. *J Mol Endocrinol* 21:109-120.
- Cazillis M, Gonzalez BJ, Billardot C, Lombet A, Fraichard A, Samarut J, Gressens P, Vaudry H, Rostene W. 2004. VIP and PACAP induce selective neuronal differentiation of mouse embryonic stem cells. *Eur J Neurosci* 19:798-808.
- Christophe J. 1993. Type I receptors for PACAP (a neuropeptide even more important than VIP?). *Biochim Biophys Acta* 1154:183-199.
- Crouch SP, Kozlowski R, Slater KJ, Fletcher J. 1993. The use of ATP bioluminescence as a measure of cell proliferation and cytotoxicity. *J Immunol Methods* 160:81-88.
- Dicicco-Bloom E, Lu N, Pintar JE, Zhang J. 1998. The PACAP ligand/receptor system regulates cerebral cortical neurogenesis. *Ann N Y Acad Sci* 865:274-289.
- Eccleston PA, Mirsky R, Jessen KR. 1991. Spontaneous immortalisation of Schwann cells in culture: Short-term cultured Schwann cells secrete growth inhibitory activity. *Development* 112:33-42.
- Gritti A, Parati EA, Cova L, Frolichsthal P, Galli R, Wanke E, Faravelli L, Morassutti DJ, Roisen F, Nickel DD, Vescovi AL. 1996. Multipotential stem cells from the adult mouse brain proliferate and self-renew in response to basic fibroblast growth factor. *J Neurosci* 16:1091-1100.
- Gross RE, Mehler MF, Mabie PC, Zang Z, Santachi L, Kessler JA. 1996. Bone morphogenetic proteins promote astroglial lineage commitment by mammalian subventricular zone progenitor cells. *Neuron* 17:595-606.
- Jamen F, Puech R, Bockaert J, Brabet P, Bertrand G. 2002. Pituitary adenylate cyclase-activating polypeptide receptors mediating insulin secretion in rodent pancreatic islets are coupled to adenylyl cyclase but not to PLC. *Endocrinology* 143:1253-1259.
- Jaworski DM, Proctor MD. 2000. Developmental regulation of pituitary adenylate cyclase-activating polypeptide and PAC(1) receptor mRNA expression in the rat central nervous system. *Brain Res Dev Brain Res* 120:27-39.
- Kaufman MH. 1998. The atlas of mouse development. London: Academic press.
- Kilpatrick TJ, Bartlett PF. 1993. Cloning and growth of multipotential neural precursors: Requirements for proliferation and differentiation. *Neuron* 10:255-265.
- Lee M, Lelievre V, Zhao P, Torres M, Rodriguez W, Byun JY, Doshi S, Ioffe Y, Gupta G, de los Monteros AE. 2001. Pituitary adenylate cyclase-activating polypeptide stimulates DNA synthesis but delays maturation of oligodendrocyte progenitors. *J Neurosci* 21:3849-3859.
- Lelievre V, Hu Z, Byun JY, Ioffe Y, Waschek JA. 2002. Fibroblast growth factor-2 converts PACAP growth action on embryonic hind-brain precursors from stimulation to inhibition. *J Neurosci Res* 67:566-573.
- Li BS, Ma W, Zhang L, Barker JL, Stenger DA, Pant HC. 2001. Activation of phosphatidylinositol-3 kinase (PI-3K) and extracellular regulated kinases (Erk1/2) is involved in muscarinic receptor-mediated DNA synthesis in neural progenitor cells. *J Neurosci* 21:1569-1579.
- Liu SY, Zhang ZY, Song YC, Qiu KJ, Zhang KC, An N, Zhou Z, Cai WQ, Yang H. 2004. SVZa neural stem cells differentiate into distinct lineages in response to BMP4. *Exp Neurol* 190:109-121.
- Lu N, DiCicco-Bloom E. 1997. Pituitary adenylate cyclase-activating polypeptide is an autocrine inhibitor of mitosis in cultured cortical precursor cells. *Proc Natl Acad Sci USA* 94:3357-3362.
- Lu N, Zhou R, DiCicco-Bloom E. 1998. Opposing mitogenic regulation by PACAP in sympathetic and cerebral cortical precursors correlates with differential expression of PACAP receptor (PAC1-R) isoforms. *J Neurosci Res* 53:651-662.
- Mabie PC, Mehler MF, Kessler JA. 1999. Multiple roles of bone morphogenetic protein signaling in the regulation of cortical cell number and phenotype. *J Neurosci* 19:7077-7088.
- Mercer A, Ronnhelm H, Holmberg J, Lundh H, Heidrich J, Zachrisson O, Ossoinak A, Frisen J, Patrone C. 2004. PACAP promotes neural stem cell proliferation in adult mouse brain. *J Neurosci Res* 76:205-215.
- Muller JM, Lelievre V, Becq-Giraudon L, Meunier AC. 1995. VIP as a cell-growth and differentiation neuromodulator role in neurodevelopment. *Mol Neurobiol* 10:115-134.
- Nadarajah B, Alifragis P, Wong RO, Parnavelas JG. 2002. Ventricle-directed migration in the developing cerebral cortex. *Nat Neurosci* 5:218-224.
- Nakashima K, Yanagisawa M, Arakawa H, Kimura N, Hisatsune T, Kawabata M, Miyazono K, Taga T. 1999. Synergistic signaling in fetal brain by STAT3-Smad1 complex bridged by p300. *Science* 284:479-482.
- Otto C, Kovalchuk Y, Wolfer DP, Gass P, Martin M, Zuschratter W, Grone HJ, Kellendonk C, Tronche F, Maldonado R. 2001. Impairment of mossy fiber long-term potentiation and associative learning in pituitary adenylate cyclase activating polypeptide type I receptor-deficient mice. *J Neurosci* 21:5520-5527.
- Panchision DM, Pickel JM, Studer L, Lee SH, Turner PA, Hazel TG, McKay RD. 2001. Sequential actions of BMP receptors control neural precursor cell production and fate. *Genes Dev* 15:2094-2110.
- Pisegna JR, Moody TW, Wank SA. 1996. Differential signaling and immediate-early gene activation by four splice variants of the human pituitary adenylate cyclase-activating polypeptide receptor (hPACAP-R). *Ann N Y Acad Sci* 805:54-64. Discussion 64-66.
- Rayan GM, Said SI, Cahill SL, Duke J. 1991. Vasoactive intestinal peptide and nerve regeneration. *J Hand Surg [Br]* 16:515-518.
- Reynolds BA, Weiss S. 1996. Clonal and population analyses demonstrate that an EGF-responsive mammalian embryonic CNS precursor is a stem cell. *Dev Biol* 175:1-13.
- Reynolds BA, Tetzlaff W, Weiss S. 1992. A multipotent EGF-responsive striatal embryonic progenitor cell produces neurons and astrocytes. *J Neurosci* 12:4565-4574.
- Richards LJ, Kilpatrick TJ, Bartlett PF. 1992. De novo generation of neuronal cells from the adult mouse brain. *Proc Natl Acad Sci USA* 89:8591-8595.
- Sauvageot CM, Stiles CD. 2002. Molecular mechanisms controlling cortical gliogenesis. *Curr Opin Neurobiol* 12:244-249.
- Suh J, Lu N, Nicot A, Tatsuno I, DiCicco-Bloom E. 2001. PACAP is an anti-mitogenic signal in developing cerebral cortex. *Nat Neurosci* 4:123, 124.
- Tatsuno I, Somogyvari-Vigh A, Arimura A. 1994. Developmental changes of pituitary adenylate cyclase activating polypeptide (PACAP) and its receptor in the rat brain. *Peptides* 15:55-60.
- Toda H, Tsuji M, Nakano I, Kobuke K, Hayashi T, Kasahara H, Takahashi J, Mizoguchi A, Houtani T, Sugimoto T. 2003. Stem cell-derived neural stem/progenitor cell supporting factor is an autocrine/paracrine survival factor for adult neural stem/progenitor cells. *J Biol Chem* 278:35491-35500.
- Vallejo I, Vallejo M. 2002. Pituitary adenylate cyclase-activating polypeptide induces astrocyte differentiation of precursor cells from developing cerebral cortex. *Mol Cell Neurosci* 21:671-683.
- Vaudry D, Rousselle C, Basille M, Falluel-Morel A, Pamanung TF, Fontaine M, Fournier A, Vaudry H, Gonzalez BJ. 2002. Pituitary adenylate cyclase-activating polypeptide protects rat cerebellar granule neurons against ethanol-induced apoptotic cell death. *Proc Natl Acad Sci USA* 99:6398-6403.
- Vescovi AL, Parati EA, Gritti A, Poulain P, Ferrario M, Wanke E, Frolichsthal-Schoeller P, Cova L, Arcellana-Panlilio M, Colombo A. 1999. Isolation and cloning of multipotential stem cells from the embryonic human CNS, establishment of transplantable human neural stem cell lines by epigenetic stimulation. *Exp Neurol* 156:71-83.
- Waschek JA, Casillas RA, Nguyen TB, DiCicco-Bloom EM, Carpenter EM, Rodriguez WI. 1998. Neural tube expression of pituitary ade-

- nylate cyclase-activating peptide (PACAP) and receptor: Potential role in patterning and neurogenesis. *Proc Natl Acad Sci USA* 95: 9602-9607.
- Waschek JA, Diccio-Bloom EM, Lelievre V, Zhou X, Hu Z. 2000. PACAP action in nervous system development, regeneration, and neuroblastoma cell proliferation. *Ann N Y Acad Sci* 921:129-136.
- Wislet-Gendebien S, Bruyere F, Hans G, Leprince P, Moonen G, Rogister B. 2004. Nestin-positive mesenchymal stem cells favour the astroglial lineage in neural progenitors and stem cells by releasing active BMP4. *BMC Neurosci* 5:33.
- Zhou C, Kikuyama S, Nakajo S, Hirabayashi T, Mizushima H, Shioda S. 2000a. Splice variants of PAC(1) receptor during early neural development of rats. *Peptides* 21:1177-1183.
- Zhou CJ, Kikuyama S, Shibayama M, Hirabayashi T, Nakajo S, Arimura A, Shioda S. 2000b. Cellular distribution of the splice variants of the receptor for pituitary adenylate cyclase-activating polypeptide (PAC(1)-R) in the rat brain by in situ RT-PCR. *Brain Res Mol Brain Res* 75:150-158.
- Zhou CJ, Shioda S, Yada T, Inagaki N, Pleasure SJ, Kikuyama S. 2002. PACAP and its receptors exert pleiotropic effects in the nervous system by activating multiple signaling pathways. *Curr Protein Pept Sci* 3:423-439.
- Zhou CJ, Yada T, Kohno D, Kikuyama S, Suzuki R, Mizushima H, Shioda S. 2001. PACAP activates PKA, PKC and Ca(2+) signaling cascades in rat neuroepithelial cells. *Peptides* 22:1111-1117.



## Solo/Trio8, a Membrane-Associated Short Isoform of Trio, Modulates Endosome Dynamics and Neurite Elongation

Ying-Jie Sun,<sup>1,5†</sup> Kaori Nishikawa,<sup>1,3†</sup> Hideki Yuda,<sup>1</sup> Yu-Lai Wang,<sup>1</sup> Hitoshi Osaka,<sup>3</sup>  
Nobuna Fukazawa,<sup>1,4</sup> Akira Naito,<sup>5</sup> Yoshihisa Kudo,<sup>4</sup>  
Keiji Wada,<sup>1,7</sup> and Shunsuke Aoki<sup>1,2,6,7\*</sup>

Department of Degenerative Neurological Diseases<sup>1</sup> and Department of Demyelinating Disease and Aging,<sup>2</sup> National Institute of Neuroscience, NCNP, Kodaira, Tokyo 187-8502, Japan; Japan Science and Technology Agency (JST), Kawaguchi, Saitama 332-0012, Japan<sup>3</sup>; Laboratory of Cellular Neurobiology, Tokyo University of Pharmacology and Life Science, Hachioji, Tokyo 192-0392, Japan<sup>4</sup>; Department of Anatomy and Structural Science, Yamagata University School of Medicine, Yamagata 990-9585, Japan<sup>5</sup>; New Energy and Industrial Technology Development Organization (NEDO), Kawasaki, Kanagawa 212-8554, Japan<sup>6</sup>; and JST, CREST, Kawaguchi, Saitama 332-0012, Japan<sup>7</sup>

Received 28 December 2005/Returned for modification 15 February 2006/Accepted 28 June 2006

With DNA microarrays, we identified a gene, termed *Solo*, that is downregulated in the cerebellum of Purkinje cell degeneration mutant mice. *Solo* is a mouse homologue of rat *Trio8*—one of multiple *Trio* isoforms recently identified in rat brain. *Solo/Trio8* contains N-terminal *sec14*-like and spectrin-like repeat domains followed by a single guanine nucleotide exchange factor 1 (GEF1) domain, but it lacks the C-terminal GEF2, immunoglobulin-like, and kinase domains that are typical of *Trio*. *Solo/Trio8* is predominantly expressed in Purkinje neurons of the mouse brain, and expression begins following birth and increases during Purkinje neuron maturation. We identified a novel C-terminal membrane-anchoring domain in *Solo/Trio8* that is required for enhanced green fluorescent protein-*Solo/Trio8* localization to early endosomes (positive for both early-endosome antigen 1 [EEA1] and Rab5) in COS-7 cells and primary cultured neurons. *Solo/Trio8* overexpression in COS-7 cells augmented the EEA1-positive early-endosome pool, and this effect was abolished via mutation and inactivation of the GEF domain or deletion of the C-terminal membrane-anchoring domain. Moreover, primary cultured neurons transfected with *Solo/Trio8* showed increased neurite elongation that was dependent on these domains. These results suggest that *Solo/Trio8* acts as an early-endosome-specific upstream activator of Rho family GTPases for neurite elongation of developing Purkinje neurons.

Endosomal membrane trafficking in neurons plays a key role in various neural processes, including neurite elongation (19, 33), synaptic transmission (17), neuronal degeneration (36), and neuronal cell death or survival (7). The early endosome regulates the selective transfer of membrane proteins to other organelles, and thus it is a key organelle for sorting vesicles containing cell surface membrane proteins, including receptors, transporters, channels, and cell adhesion molecules (2, 29, 39, 47).

Several lines of evidence suggest that small GTPases play pivotal roles in regulating early-endosome dynamics (2, 39, 47). For example, Rab5 regulates the motility and fusion of early endosomes (32), whereas Rab4 and Rab5 control vesicle influx and efflux, respectively, in the early-endosome pool (28). Rho family GTPases also regulate early-endosome dynamics. Once such GTPase, Cdc42, controls endocytic transport in polarized cells (20), whereas RhoD specifically localizes to early endosomes and regulates their motility via diaphanous-related formin proteins (13). Upstream regulators of small GTPases that associate with early endosomes have been studied exten-

sively. For example, early-endosome antigen 1 (EEA1) acts as an effector for Rab family small GTPases (5, 45). Although Rho family GTPases are also activated by multivalent upstream effectors (42), the specialized upstream activators that function in early endosomes remain unknown.

*Trio*, a member of the Dbl homology domain family of guanine nucleotide exchange factors (GEFs), was originally identified by its interaction with the leukocyte common antigen-related protein receptor (6). *Trio* has an N-terminal *sec14*-like domain, spectrin-like repeats, two GEF domains (GEF1 and GEF2), an immunoglobulin (Ig)-like domain, and a C-terminal Ser/Thr kinase domain (3). The GEF1 domain activates RhoG and Rac1, whereas GEF2 acts on RhoA, suggesting that *Trio* is involved in multiple GTPase cascades mediating various cellular processes (3). Genetic analysis of the *Trio* gene in *Drosophila* embryos implicates this protein in neuronal and retinal axon guidance (3). Mice lacking *Trio* die during embryogenesis and exhibit a loss of myofiber formation and cellular disorganization in the hippocampus and olfactory bulb (35). Although *Trio* is highly expressed in the adult brain, heart, liver, skeletal muscle, kidney, placenta, and pancreas (6), its effector function in these adult tissues remains unknown. Several *Trio* isoforms were recently identified (25), and the expression of each isoform was shown to be regulated in a tissue-specific manner. The functions of these isoforms, however, have not been delineated.

Purkinje cell degeneration (*pcd*) is an autosomal recessive

\* Corresponding author. Mailing address: Department of Degenerative Neurological Diseases, National Institute of Neuroscience, National Center of Neurology and Psychiatry, 4-1-1 Ogawahigashi, Kodaira, Tokyo 187-8502, Japan. Phone: 81-42-346-1715. Fax: 81-42-346-1745. E-mail: aokis@ncnp.go.jp.

† Y.-J.S. and K.N. contributed equally to this work.

mutational disorder in mice that is characterized by degenerative loss of Purkinje neurons after postnatal day 15 (P15) to P18 (30). The causative mutation of *pcd* was identified at the *Nnal1* locus (12). The disorder constitutes an adult-onset disease and presents mild phenotypes, thereby facilitating the analysis of cerebella that are nearly devoid of Purkinje neurons. Thus, the *pcd* mouse has been repeatedly used to screen for Purkinje neuron-specific genes, such as the gene encoding 28-kDa calbindin (34) or inositol 3-phosphate receptor 1 (IP3R) (24).

In this study, we used DNA microarrays to analyze gene expression in the cerebella of mice carrying a mutation governing *pcd* (30). We identified a Purkinje-predominant mouse cDNA encoding the protein Solo, which is a membrane-associated isoform of Trio. Amino acid sequence analysis showed that Solo is a homologue of the recently identified rat protein Trio8 (25). Solo/Trio8 specifically localized to early endosomes and regulated their dynamics. We also found that Solo/Trio8 modulated neurite morphology in primary cultured neurons. These data suggest that Solo/Trio8 is involved in the development of Purkinje neurons by affecting the dynamics of early endosomes.

#### MATERIALS AND METHODS

**Animals.** C57BL/6J-*pcd* mice were obtained from The Jackson Laboratory (Bar Harbor, ME). The cerebella of P24 *pcd* and wild-type (WT) mice were used for DNA microarrays. For SYBR green-based real-time quantitative reverse transcription (RT)-PCR, three cerebella were collected on each postnatal day. Animal care and handling were in accordance with institutional regulations for animal care and public law and were approved by the Animal Investigation Committee of the National Institute of Neuroscience, Japan.

**DNA microarrays.** Equivalent amounts of total RNA derived from each cerebellar sample were reverse transcribed into double-stranded cDNA that was then used as a template to synthesize biotin-labeled cRNA with the BioArray HighYield RNA transcription labeling kit (Enzo Diagnostics, Farmingdale, NY). Labeled cRNA was purified on RNeasy affinity resin (QIAGEN, Valencia, CA) and fragmented randomly to an average size of 50 to 100 bases by incubation in 40 mM Tris-acetate, pH 8.2, containing 100 mM K-acetate and 30 mM Mg-acetate at 94°C for 35 min. The labeled cRNA samples were analyzed with the Affymetrix murine genome U74A, -B, and -C array set (Affymetrix, Santa Clara, CA). Hybridization and array scanning were performed according to protocols provided by Affymetrix. Data analysis was performed with Microarray Suite software (Affymetrix).

**5' RACE.** 5' rapid amplification of cDNA ends (RACE) was performed with the 5' RACE kit (Invitrogen, Carlsbad, CA) according to the manufacturer's protocol. First-strand cDNA was synthesized from cerebellar total RNA with a gene-specific primer (5'-AGAAACCAAAATGAGGCTGCTA-3') corresponding to the cDNA sequence of expressed sequence tag (EST) clone A1587721. Nested PCR was performed to amplify DNA between the anchor primer and another primer (5'-TGAGGCTGCTAAGAATGGCTTGACTG-3') specific for A1587721. The product (~1.2 kbp) displayed strong homology to the Trio cDNA sequence (GenBank accession no. NM\_007118). A cDNA encoding the Solo/Trio8 open reading frame (ORF) was obtained by RT-PCR with primers 5'-TC TCGAGATGAAAGCTATGGATGTTTCC-3' and 5'-AGAATTCGAATG GAAAGGTAAGGAACTGAG-3', derived from the human Trio gene (GenBank accession no. NM\_007118) and the 1.2-kbp product, respectively. The resulting 5.6-kbp Solo/Trio8 DNA fragment was subcloned into the pGEM-T Easy vector (Promega, Madison, WI) for further sequencing.

**In situ hybridization.** In situ hybridization was performed as described previously (1). To synthesize cRNA probes for the Trio gene, the 357-bp fragment encoding part of the Solo gene (nucleotides [nt] 5134 to 5490; DDBJ accession no. AB106872; common probe) and a 339-bp noncoding part of the Solo gene (nt 5606 to 5944; Solo-specific probe) were subcloned into pBluescript-SKII (+) (Stratagene, La Jolla, CA).

**SYBR green-based real-time quantitative RT-PCR.** SYBR green-based real-time quantitative RT-PCR was performed with primers 5'-TCTCTCAGACAG ACAGCCACGT-3' (forward) and 5'-TGCTTCATATTAAGGGCAGCAG-3'

(reverse) to amplify Solo/Trio8 cDNA and primers 5'-AGAAGTGGTGAAG CAGGCAT-3' (forward) and 5'-ATCGAAGTGGAAAGCTGGGA-3' (reverse) for glyceraldehyde-3-phosphate dehydrogenase (GAPDH) cDNA. The quantitative RT-PCR method (user bulletin 2; Applied Biosystems, Foster City, CA) was modified to establish an expression level index for mRNA (1).

**Plasmid constructs.** With mouse cerebellar cDNA as a template, we performed PCR to construct plasmids encoding full-length (amino acids [aa] 1 to 1849) Solo/Trio8 tagged (N or C terminally) with enhanced green fluorescent protein (EGFP) and FLAG; Solo/Trio8 mutant constructs lacking the C-terminal transmembrane domain [Solo-TM(-) aa 1 to 1830; DDBJ accession no. AB106872] were prepared similarly. The primers used were 5'-CCGCTCGAG ATGAAAGCTATGGATGTTTGGCC-3' [forward primer for N- or C-terminally EGFP-tagged Solo and EGFP-Solo-TM(-)], 5'-GGAATTCGAATGGA AAGTAAGGAAACTGAGC-3' (reverse primer for EGFP-Solo), 5'-GGAA TTCGCTGTCATCTCGAGTCCGGCTGA-3' [reverse primer for EGFP-Solo-TM(-)], 5'-CCGCTCGAGCGATGACTACAAGGACGACGAT GACAAGATGAAAGCTATGGATGTTTGGCA-3' [forward primer for N-terminally FLAG-tagged Solo and FLAG-Solo-TM(-)], 5'-GGGGGCGCGCC CTCAAATGAAAGGTAAGGAAACT-3' (reverse primer for N-terminally FLAG-tagged Solo), 5'-GGGGGCGCGCCCTCACTGTCATCTCGAGT CCG-3' [reverse primer for N-terminally FLAG-tagged Solo-TM(-)], 5'-CCG CTCGAGATGGATGAAAGCTATGGATGTTTGGC-3' [forward primer for C-terminally FLAG-tagged Solo and FLAG-Solo-TM(-)], 5'-GGGGGCGCGC CGCTTACTGTCATCTCGCTGCTGTAGTCAATGAAAGGTAAGGA AACTGAGC-3' (reverse primer for C-terminally FLAG-tagged Solo), 5'-GGG GCGCGCGCTTACTGTCATCTCGCTGCTGTAGTCAATGTCATCTCGCT GCGAGTCCGGCTG-3' [reverse primer for C-terminally FLAG-tagged Solo-TM(-)]. *Pfu* DNA polymerase was used for PCR, and the amplified products were cloned between the XhoI and EcoRI sites of pEGFP-C3/pEGFP-N1 (Clontech, Palo Alto, CA) or the XhoI and NotI sites of pCI-neo (Promega). To construct the GEF1-inactivated Solo mutant form Solo-AE, the mutations Gln<sup>1368</sup> to Ala and Leu<sup>1378</sup> to Glu were introduced into EGFP-Solo with the QuikChange site-directed mutagenesis kit (Stratagene) and primers 5'-CAAA CAGTTGCCCGGATAACAAAGATACAGCTCGAGTTAAAGGAG-3' and 5'-CTCCTTAACTCGAGCTGATACCTTTTATCCGGGCAACTGGT TT G-3'. All gene constructs were confirmed by DNA sequencing. Expression of the genes for Solo/Trio8 was controlled with a cytomegalovirus promoter.

**Cell culture and transient transfections.** COS-7, HEK293T, and NIH 3T3 cells were cultured at 37°C in 5% CO<sub>2</sub> in Dulbecco modified Eagle medium containing 10% fetal bovine serum, 100 U/ml penicillin, and 85 µg/ml streptomycin (Invitrogen). Cells were grown on 6- and 24-well or 100-mm dishes and four- and eight-well chamber slides and transfected with equal amounts (0.4 to 3.0 or 20 µg) of plasmid DNA per well with the Lipofectamine 2000 DNA transfection reagent (Invitrogen) according to the manufacturer's instructions and cultured for 8 to 24 h at 37°C.

**Rac1 pull-down assay.** COS-7 cells were cultured at a density of  $2 \times 10^6$  cells per 100-mm dish and transfected with 20 µg of an EGFP-Solo expression construct or a control plasmid (pEGFP) as described above. After 16 h, cells were serum starved for 5 h and then washed with phosphate-buffered saline (PBS) and lysed in lysis buffer (25 mM HEPES, [pH 7.5], 150 mM NaCl, 1% [wt/vol] Igepal CA-630, 20 mM MgCl<sub>2</sub>, 1 mM EDTA, 2% [wt/vol] glycerol, 1 mM Na<sub>2</sub>VO<sub>4</sub>, 25 mM NaF, complete EDTA-free protease inhibitor mixture [Roche Molecular Biochemicals, Indianapolis, IN]). Cell lysates were centrifuged at 20,000 × g for 20 min at 4°C. Rac1 activation was measured with the Rac1 activation assay kit (Upstate Biotechnology Inc., Lake Placid, NY) according to the manufacturer's instructions. Briefly, 0.5 ml of the supernatant (2 mg protein) was added to 10 µl of PAK1-p21-binding domain (PBD)-glutathione S-transferase-glutathione agarose beads (Upstate Biotechnology, Inc.), and the mixture was rotated for 1 h at 4°C, followed by three washes of the protein complexes with lysis buffer. PAK1-PBD-bound proteins were dissociated and denatured by boiling in Laemmli sample buffer and subjected to sodium dodecyl sulfate-polyacrylamide gel electrophoresis. The amount of active Rac1 (GTP-bound form) was analyzed by immunoblotting with a monoclonal antibody to Rac1 (Upstate Biotechnology, Inc.).

**Cell fractionation.** COS-7 cells were transfected with expression plasmids and cultured for 24 h. The cells were homogenized in 300 µl of ice-cold TNE buffer (50 mM Tris-HCl [pH 7.5], 150 mM NaCl, 1 mM EDTA) supplemented with protease inhibitors (Complete Protease Inhibitors; Roche Molecular Biochemicals) and sonicated for 30 s on ice. The homogenates were subjected to centrifugation at 20,000 × g for 30 min at 4°C. Supernatants (cytoplasmic fraction) were pooled, and pellets (including light membranes) were washed twice with 0.5 ml of TNE buffer and then lysed for 30 min on ice in radioimmunoprecipitation assay buffer (50 mM Tris-HCl [pH 7.5], 150 mM NaCl, 1 mM EDTA, 0.5%

sodium deoxycholate, 0.1% sodium dodecyl sulfate) with protease inhibitors and subjected to centrifugation at 20,000  $\times$  g for 30 min at 4°C.

**Western blotting.** Western blotting was performed as described previously (1). Blots were probed with antibodies to detect EGFP (anti-Living Colors A.v., JL-8; Clontech), anti-FLAG M2 (Sigma, St. Louis, MO), anti-I $\kappa$ B (Cell Signaling Technology, Beverly, MA), anti-platelet-derived growth factor (PDGF) receptor  $\alpha/\beta$  (Upstate Biotechnology, Inc.) or anti- $\beta$ -actin (Sigma).

**Neuronal cultures and transfections.** Fetal C57BL/6J mice at embryonic day 16 (E16) were used for the primary culture of embryonic cortical neurons. The brain of each embryo was dissected from the overlying meninges, blood vessels, olfactory bulb, and hippocampus in Hanks' balanced salt solution (HBSS; Gibco, Gaithersburg, MD). Brains were minced with a 0.1-mm blade, and small pieces of the tissues were incubated in 0.25% trypsin-0.04% EDTA (Gibco) for 10 min at 37°C. Digestion was stopped by addition of 2% fetal bovine serum, and the mixture was incubated with 0.01% DNase I (Sigma) at room temperature for 2 min. After being spun down (5 min at 280  $\times$  g), neuronal cells were resuspended in HBSS. Single-cell suspensions were obtained by trituration and filtered through a 70- $\mu$ m nylon cell strainer (BD, Bedford, MA) to remove undigested cell aggregates, followed by centrifugation for 5 min at 280  $\times$  g. Dispersed neurons were plated on Biotin-coated poly-D-lysine-coated four-well chamber slides (BD) at a density of  $2 \times 10^5$  or  $4 \times 10^5$  cells per well in Neurobasal medium (Invitrogen) containing B27 supplement (Invitrogen), penicillin-streptomycin (Invitrogen), and 2 mM L-glutamine (Invitrogen). The cultures were maintained at 37°C in a 5% CO<sub>2</sub> humidified incubator, and half of the medium volume was replaced with fresh medium about every 2 days. Cortical neurons were grown for 6 days in culture and then transfected as described above. For cotransfections, Lipofectamine 2000 reagent (4  $\mu$ l) and DNA (a total of 1.6  $\mu$ g of plasmids containing EGFP or EGFP-fused protein and DsRed [pDsRed Express-C1; Clontech] at a ratio of 8:1) were separately suspended in Opti-MEM (50  $\mu$ l; Invitrogen) and gently combined. After a 20-min incubation at room temperature, the mixture (100  $\mu$ l) was added to the culture medium (400  $\mu$ l). DsRed is used to visualize the morphology of the transfected neurons (41). Neurons were allowed to express the transfected protein for 18 h, fixed with 4% formaldehyde in PBS, and immunostained with polyclonal anti-DsRed (1:10,000; rabbit IgG; BD) and mouse monoclonal anti-GFP 3E6 (1:2,000; Molecular Probes, Eugene, OR). Alexa Fluor dye-conjugated secondary antibodies (1:400; Molecular Probes) were used.

**Immunofluorescence microscopy.** Fluorescence immunostaining was performed as described previously (1). Dilutions of primary antibodies were as follows: anti-EEA1, anti-Bip/GRP78, and anti-GM130 (from BD Biosciences), all 1:100; anti-Rab5a and anti-Rab5b (Santa Cruz Biotech, Santa Cruz, CA), 1:200; anti-Rab7 (Santa Cruz Biotech), 1:100; anti-Tau1 and anti-Map2 (Chemicon International, Temecula, CA), 1:200; anti-calbindin D28k (Swant, Bellinzona, Switzerland), 1:500. All Alexa Fluor dye-conjugated secondary antibodies (Molecular Probes) were diluted 1:200. Immunofluorescence microscopy was performed with an ORCA-ER digital camera (Hamamatsu Photonics, Hamamatsu, Japan), and confocal microscopy was performed with the FLUOVIEW system (Olympus, Tokyo, Japan) or the Leica TCS SP2 spectral confocal scanning system (Leica Microsystems, Wetzlar, Germany) with a 20 $\times$  objective lens, and images were acquired with Leica Confocal Software version 2.5.

**Measurement of EEA1-positive vesicles.** For analysis of early endosomes, the number of EEA1-positive vesicles in COS-7 cells expressing EGFP chimeras (and containing an intact nucleus stained with 4',6'-diamidino-2-phenylindole [DAPI]) was quantified with Image-Pro Plus software version 4.5.1 (Media Cybernetics, Silver Spring, MD). EEA1-positive vesicles ( $>0.04 \mu\text{m}^2$ ) were assayed by counting 40 cells. After we extracted the morphology of EEA1-positive endosomes with the object-extracting module of Image-Pro Plus, the clustered vesicles were separated with the Watershed Split module in the software. These data were statistically analyzed with Prism software version 3.0c (GraphPad, San Diego, CA). The data were statistically evaluated with one-way analysis of variance, followed by Bonferroni's test.

**Endocytosis.** Transferrin or Sulforhodamine 101 uptake was assessed as described previously (14, 50). Briefly, COS-7 cells were transfected with EGFP or EGFP-Solo constructs by using Lipofectamine 2000. Seven hours after transfection, the cells were depleted of bovine transferrin by incubation for 45 min in Dulbecco modified Eagle medium containing 0.1% bovine serum albumin and then labeled with human transferrin fluorescently labeled with Alexa-594 (Molecular Probes) at 25  $\mu\text{g}/\text{ml}$  or with the fluid-phase fluorescent marker Sulforhodamine 101 (Molecular Probes) at 25  $\mu\text{g}/\text{ml}$  for 15 min at 37°C. Internalization was then stopped by placing the cells on ice and washing them three times with ice-cold PBS before formaldehyde fixation. For analysis of endocytosis, fluorescence of Alexa-594-labeled transferrin or Sulforhodamine 101 in COS-7

cells expressing EGFP-Solo chimeras was quantified with Image-Pro Plus software version 4.5.1 with the density histogram module.

**Cortical neuron morphometry and analysis.** Images of immunostained neurons as described above were captured with an ORCA-ER digital camera, and morphometric analysis of the neurites and their branching was performed with Kurabo Neurocyte Image Analyzer software version 1.5 (KURABO, Osaka, Japan). To analyze the effects on neurite morphology, EGFP-positive cells were assayed by counting at least 60 cells from randomly selected fields. All neurites were measured irrespective of whether they were axons. Neuronal morphology was assessed according to four criteria, pass (number of branches), joint (number of branch points), total length (axon-and-dendrite length), and average maximum neurite length (axon length; Tau1 immunohistochemistry showed that the longest neurite of E16 mouse-derived embryonic cortical neurons was an axon; data not shown). The data were statistically evaluated by one-way analysis of variance, followed by Bonferroni's test.

**Organotypic slice culture.** The method used for slice culture has been described previously (49). In brief, C57BL/6J mice were decapitated and their brains were dissected and sliced in ice-cold HBSS with a vibratome. P11 cerebella were sliced coronally at a 200- $\mu$ m thickness. Slices were transferred onto Millicell-CM inserts (Millipore, Bedford, MA) and cultured at the air-medium interface in 5% CO<sub>2</sub> in air at 37°C. Cerebellar slices were cultured essentially as described before (48), in a medium which consisted of 15% heat-inactivated horse serum (Invitrogen), 25% Earle's balanced salt solution (Sigma), 60% Eagle's basal medium (Invitrogen), 5.6 g/liter glucose, 3 mM L-glutamine, 20 nM progesterone, 1 mM sodium pyruvate, 100 U/ml penicillin, 100  $\mu\text{g}/\text{ml}$  streptomycin, and Sigma 1-1884 supplement (giving final concentrations of 5  $\mu\text{g}/\text{ml}$  insulin, 5  $\mu\text{g}/\text{ml}$  transferrin, and 5 ng/ml sodium selenite). At 1 day in vitro, cerebellar slices were transfected with small interfering RNA (siRNA).

**Transfection of siRNA.** We used siRNA to knock down Solo/Trio8 expression in cerebellar-slice cultures. A 21-oligonucleotide siRNA duplex was designed by the siDirect program (RNAi Co., Ltd., Tokyo, Japan). The siRNA oligonucleotide sequences that were used to target the C-terminal transmembrane domain in Solo/Trio8 (region, bp 5483 to 5505) were 5'-GACAAGCAUACGUUGA UUUUG-3' (sense) and 5'-AAUCAACGUAUUGCUUGUCAU-3' (antisense) and were synthesized by RNAi Co., Ltd. For the control, scrambled siRNA, silencer negative control no. 1 siRNA (proprietary sequence; Ambion, Austin, TX) was used. To confirm the siRNA effect, the EGFP-Solo plasmid and siRNA targeting Solo/Trio8, as well as a scrambled siRNA control, were cotransfected into COS-7 cells with Lipofectamine 2000 according to the manufacturer's instructions. After 24 h, significant siRNA-mediated suppression of Solo/Trio8 expression was detected by immunocytochemistry with anti-GFP monoclonal antibody 3E6 to estimate the fluorescence intensity of EGFP-expressing cells by fluorescence microscopy. For analysis of the inhibitory efficiency of siRNA, fluorescence signals in COS-7 cells expressing EGFP-Solo were quantified with Image-Pro Plus software version 4.5.1 with the density histogram module. To knock down endogenous Solo/Trio8 expression in Purkinje cells, at 1 day in vitro the siRNA was transfected into cerebellar slices with X-tremeGENE siRNA Transfection Reagent (Roche Applied Science) according to the manufacturer's instructions. In addition, scrambled siRNA no. 1 was transfected as a negative control. After 2 days, the slices were immunostained with anti-calbindin D28k as described below.

**Immunohistochemistry.** For Purkinje neuron morphometry, Purkinje cells were visualized by immunostaining with a mouse monoclonal antibody against calbindin D28k. The immunostaining method for brain slices has been described previously (48). Briefly, slices were fixed in 4% paraformaldehyde in PBS for 1 h at room temperature and washed three times with PBS. Slices were incubated with 10% normal goat serum in PBS containing 0.3% Triton X-100 for 1 h. Slices were then incubated overnight at 4°C with primary antibody diluted 1:500 in PBS containing 3% normal goat serum and 0.3% Triton X-100 and then washed three times with PBS. Slices were incubated with goat Alexa 488-conjugated secondary antibody diluted 1:200 in PBS containing 1% goat serum and 0.3% Triton X-100 for 1 h at room temperature and washed three times with PBS. Images of immunostained Purkinje neurons were captured with the Leica TCS SP2 spectral confocal scanning system (20 $\times$  objective lens), and morphometric analysis of the axons was performed with the Kurabo Neurocyte Image Analyzer as described above.

**Nucleotide sequence accession number.** The nucleotide sequence of mouse Solo/Trio8 has been deposited in the DDBJ nucleotide sequence database under accession number AB106872.

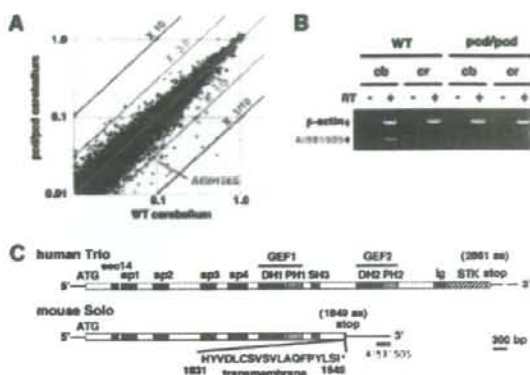


FIG. 1. Identification of a cDNA sequence predominantly expressed in Purkinje neurons. (A) Scattergram analysis of microarray data. Cerebellar cDNAs derived from pcd and WT mice were analyzed with DNA microarrays, and the average signal from each gene was normalized to the GAPDH signal and plotted to yield the scattergram. The AI591505 cDNA is indicated on the plot. (B) RT-PCR analysis of AI591505 transcript expression in the cerebella (*cb*) and cerebra (*cr*) of pcd and WT mice, respectively. PCRs for the  $\beta$ -actin gene (internal control) and AI591505 were performed in a single tube. (C) Structural relationship between the gene for Solo/Trio8 and a consensus of human Trio genes. Protein domains are indicated within the bars, and the 5' and 3' noncoding regions are indicated by horizontal lines. The domains shown are as follows: sec14, sec14p-like putative lipid binding domain; sp, spectrin-like domain; DH, Dbl homology domain; PH, pleckstrin homology domain; SH3, Src homology 3 domain; Ig, Ig-like domain; STK, serine/threonine kinase domain.

## RESULTS

**DNA microarray analysis of the pcd mouse cerebellum.** Since no exhaustive gene expression analysis of the pcd mouse has been reported to date, we evaluated changes in cerebellar gene expression from P24 pcd mice (with 70 to 80% Purkinje neuronal loss) and WT mice with DNA microarrays containing almost 6,000 characterized genes and 30,000 ESTs. A comparison between two pcd mice and two WT mice revealed pcd-specific variability in gene expression (Fig. 1A). A scattergram constructed from hybridization data of 12,518 highly expressed genes (those having signals  $>0.01\%$  of that measured for GAPDH) revealed only six upregulated genes ( $>3$ -fold) and 26 downregulated genes ( $<0.33$ -fold) in pcd mice (Table 1).

**EST AI591505 is expressed exclusively in Purkinje neurons.** Among the downregulated genes, we identified uncharacterized EST clone AI591505 (GenBank) (Fig. 1A; Table 1). AI591505 is 236 bp in length and has no homology with any annotated genes. The as-yet-uncharacterized AI591505 transcript was highly expressed in the normal mouse cerebellum ( $\sim 10\%$  of the GAPDH signal in the WT array; Fig. 1A). AI591505 was of interest because its decreased expression level in the pcd cerebellum suggested that it is a relatively highly expressed uncharacterized Purkinje neuron-specific gene. The decreased expression of the AI591505 transcript in the pcd cerebellum was confirmed by RT-PCR analysis with the cerebra and cerebella of pcd and WT mice, respectively. This transcript was expressed predominantly in the cerebellum, and expression in the pcd mouse was clearly lower than in the WT

mouse (Fig. 1B). In situ hybridization showed that the transcript was expressed predominantly in the WT Purkinje cell layer at P24 (Fig. 2B) but not in the E16 brain (Fig. 2A) and was decreased in pcd Purkinje cells (Fig. 2B, c to i). Relatively low-level expression was also detected in the olfactory bulb and hippocampus (Fig. 2B, c to e). The expression level of the AI591505 gene in the P7 pcd cerebellum (before onset of degenerative loss of Purkinje neurons) was equivalent to that in the P7 WT cerebellum (data not shown), although the *Nnal* (pcd causative gene) expression level was significantly decreased in the P7 pcd cerebellum (data not shown), suggesting that the AI591505 gene is not a downstream gene directly controlled by *Nnal* expression.

**Identification of Solo/Trio8, a Trio splice variant, expressed predominantly in Purkinje neurons.** An additional search of databases identified another EST, AI587721, containing a region overlapping the AI591505 sequence. 5' RACE with the AI587721 sequence yielded a 1.2-kbp cDNA clone from the cerebellum. A search of GenBank revealed that this clone contained a part of the *Trio* sequence (accession no. NM\_007118). To clone the entire ORF, a PCR was performed with primers for *Trio* (forward) and the cDNA clone (reverse)

TABLE 1. Genes with altered expression in the pcd cerebellum

Gene (accession no.)	Relative expression		pcd/WT ratio
	WT <sup>a</sup>	pcd <sup>a</sup>	
<b>Genes upregulated in pcd cerebellum</b>			
CPP32 (U63720)	0.042	0.137	3.29
TYRO (AF024637)	0.027	0.088	3.25
Slp-w7 (X06454)	0.024	0.082	3.45
UN <sup>b</sup> (AK084804)	0.015	0.046	3.08
UN <sup>b</sup> (BC055829)	0.014	0.043	3.00
DnaJ-like (AK053156)	0.011	0.036	3.37
<b>Genes downregulated in pcd cerebellum</b>			
IP3R1 (X15373)	0.533	0.054	0.10
28-kDa calbindin (D26352)	0.525	0.032	0.06
NK6 (AK083449)	0.396	0.113	0.29
PCP-1 (M21530)	0.356	0.040	0.11
RG88 (AK044337)	0.322	0.084	0.26
GluR1 (BC056397)	0.299	0.098	0.33
PCP-2 (M21532)	0.298	0.056	0.19
DRR1-like (AK032875)	0.162	0.040	0.24
Ca <sup>2+</sup> -ATPase (BC026147)	0.146	0.019	0.13
PKC- $\gamma$ (L28035)	0.135	0.024	0.18
EAAC4 (D83262)	0.131	0.017	0.13
MGF (M57647)	0.129	0.031	0.24
Delphilin (AF099933)	0.127	0.013	0.10
rp S18a (AB049953)	0.114	0.031	0.27
AI591505	0.094	0.028	0.30
Tubulin ligase (AB093278)	0.087	0.014	0.16
Metalloprotease (AK034528)	0.074	0.023	0.31
Shank2 (AB099695)	0.066	0.019	0.28
PH protein (AK028383)	0.060	0.013	0.22
NSC dendrite regulator (BC030853)	0.056	0.017	0.31
Aspartate- $\beta$ -hydroxylase (AF289488)	0.056	0.017	0.31
Ca <sup>2+</sup> channel $\alpha$ 1G (AJ012569)	0.055	0.011	0.20
Tm4sf10 (BC019751)	0.049	0.015	0.31
Chemokine (AY241872)	0.039	0.013	0.32
Oxytocin-neurophysin I (M88355)	0.038	0.011	0.28
ARM repeat protein (AK044219)	0.033	0.010	0.30

<sup>a</sup> Expression level relative to GAPDH (average from two WT or pcd mice).  
<sup>b</sup> UN, uncharacterized gene.

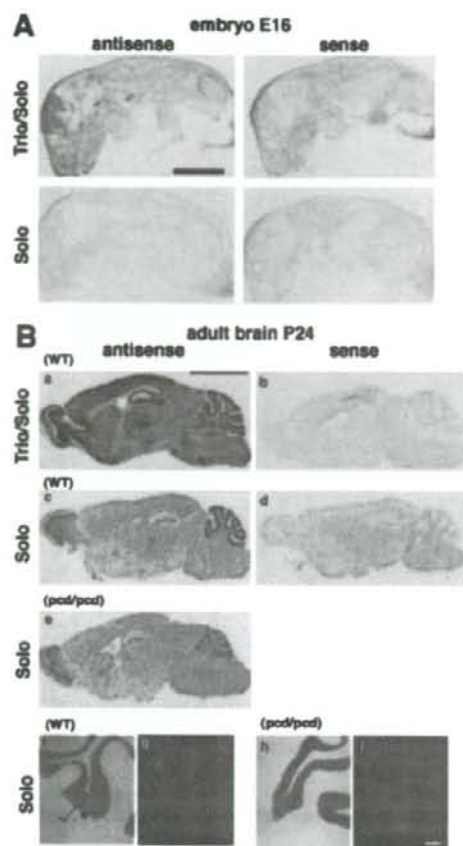


**FIG. 2.** Expression of Solo and Trio mRNAs in the mouse embryo and adult mouse brain. (A) In situ hybridization analysis of the mouse embryo (E16) with Solo-specific and Solo/Trio-common cRNA probes. Antisense and sense probes were prepared with Solo-specific and Solo/Trio (common to both) regions of the cDNA, respectively, and hybridized with tissue sections from an E16 mouse whole embryo. Bar = 5 mm. (B) In situ hybridization analysis of Solo transcript (AI591505) in P24 WT (a to d, f, g) and *pod* (e, h, i) brains. Antisense and sense probes were prepared from Solo-specific and Solo/Trio (common to both) regions of the cDNA, respectively, and hybridized with tissue sections from P24 mouse whole brains. Regions in part a are labeled as follows: cb, cerebellum; ctx, cortex; hp, hippocampus; ob, olfactory bulb. The arrow in part f indicates the Purkinje cell layer, and the bars in part f indicate the molecular (lower) and granule (upper) layers. Bar in part a = 5 mm (same scale for parts a to e). Bar in part i = 200  $\mu$ m (same scale for parts f to i).

to yield a cDNA with an entire ORF of 5,550 bp encoding 1,849 aa (Fig. 1C) from the cerebellum. The human *Trio* ORF contains 8,586 bp encoding 2,861 aa (6) (Fig. 1C); the cloned cDNA lacked the region between nucleotides 5491 and 8586 but contained a distinct 874-bp sequence at the 3' end (Fig. 1C). A search of GenBank revealed the corresponding exon in the mouse *Trio* gene (data not shown), suggesting that the transcript is an alternatively spliced product of the *Trio* gene. We thus named this isoform Solo, for short-form splice variant

of *Trio*. Solo contains an N-terminal sec14-like domain, spectrin-like repeats, a GEF1 domain, one SH3-like domain, and the unique C-terminal hydrophobic sequence HYVDLCSVS VLAQFPYLSI (aa 1831 to 1849, Fig. 1C). Computational analyses with a protein motif search program (<http://motif.genome.ad.jp/>) suggested that this C-terminal hydrophobic sequence resembles transmembrane helices of G-protein-coupled receptors (data not shown). McPherson et al. recently reported identification of rat Trio variants (25). Among them, the amino acid sequence of rat Trio8 was highly similar (99.7%) to that of mouse Solo, suggesting that Solo is a mouse homologue of Trio8.

To delineate the expression patterns of the genes for Solo/Trio8 and Trio in the mouse brain, we performed in situ hybridization with Solo-specific and Solo/Trio-common cRNA probes. The Solo/Trio-common probe signal was distributed over the entire mouse brain, and more-intense signals were observed in the hippocampus, olfactory bulb, cortical layers, and cerebellum (Fig. 2B, a and b). This hybridization pattern differed from that of the Solo-specific probe, which was predominantly expressed in the Purkinje cell layer of the cerebellum (Fig. 2B, c, d, f, and g). To determine if Solo/Trio8 mRNA is actually translated into protein, we performed Western blot analysis with a polyclonal antibody recognizing a 14-aa internal sequence near the N terminus of Solo and Trio (anti-Solo/Trio antibody). The immunoblot showed a 210-kDa immunoreactive band in the mouse cerebellum, in good agreement with the expected molecular mass of Solo (212 kDa) (data not shown). McPherson et al. (25) also detected a 210-kDa rat Trio8 protein in the rat cerebellum by Western blotting with an antibody against Trio8. The size of the Solo/Trio8 protein in mouse and rat cerebella was identical to that measured in COS-7 cells transfected with the Solo expression vector (Fig. 3C). Our antibody against Solo/Trio did not work well in immunohistochemical, immunocytochemical, and fractionation experiments (data not shown), so we were unable to determine the protein expression pattern in the brain.

**Guanine nucleotide exchange activity of Solo/Trio8 for a Rho family GTPase.** The GEF1 domain of Trio activates RhoG and Rac1, whereas GEF2 acts on RhoA (3). We addressed whether the GEF1 domain of Solo/Trio8 has guanine nucleotide exchange activity for Rac1 by a pull-down assay with the PBD of PAK1, which specifically binds to GTP-bound Rac1 (active form) but not to the inactive GDP-bound form (4). The amount of activated Rac1 in COS-7 cells transfected with the EGFP-Solo construct was markedly increased compared with that in negative control cells transfected with EGFP (Fig. 3B, top). Previous studies demonstrated that a double amino acid mutant form of Trio (Q1368A and L1376E within the GEF1 domain) completely abolishes the GEF1 activity (10, 23). The Q1368A and L1376E double mutation (EGFP-Solo-AE, Fig. 3A) abolished EGFP-Solo-mediated Rac1 activation in COS-7 cells (Fig. 3B, top). The C-terminal hydrophobic sequence (HYVDLCSVS VLAQFPYLSI; Fig. 1C) of Solo/Trio8 was predicted by a protein motif search program to function as a membrane-anchoring domain (data not shown). Deletion of this putative domain (EGFP-Solo-TM(-), Fig. 3A) did not affect Rac1 activation (Fig. 3B, top). There was no significant difference in the total amount of Rac1 expressed in COS-7 cells transfected with the EGFP, EGFP-Solo, EGFP-

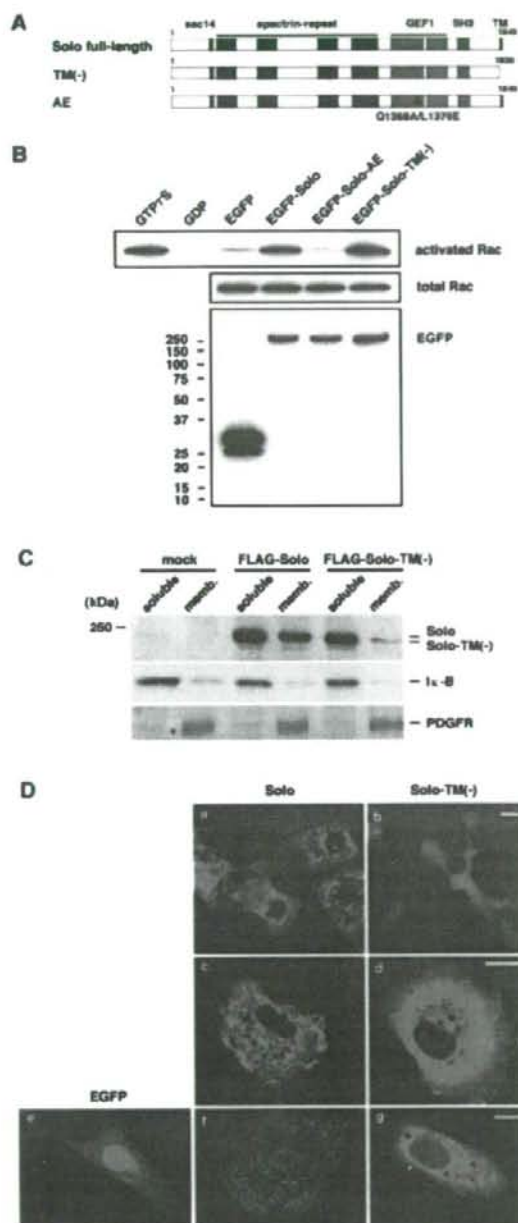


**FIG. 3.** GEF activity of Solo/Trio8 and localization in cellular membranes. (A) Schematic representation of full-length, C-terminally truncated Solo-TM(-) and AE mutant (GEF inactive; Q1368A/L1376E). (B) Rac1 activation by the GEF1 activity of Solo/Trio8. EGFP, EGFP-Solo, EGFP-Solo-AE, and EGFP-Solo-TM(-) were transiently expressed in COS-7 cells. Cells were cultured for 24 h and then serum starved for an additional 5 h prior to the Rac1 activation assay. PBD-bound Rac1 protein was pulled down and analyzed by Western blotting with monoclonal anti-Rac1. (Top) GTP-bound Rac1 (active form). Cell lysates treated with GTP $\gamma$ S or GDP served as

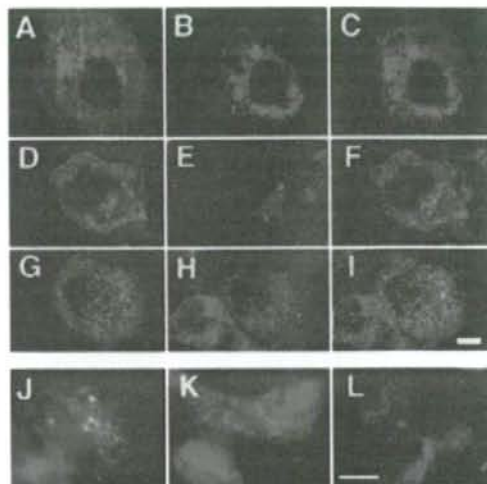


**FIG. 4.** Subcellular localization of Solo/Trio8. An EGFP-tagged Solo/Trio8 expression construct (green) was transfected into COS-7 cells (A, D, and G). COS-7 cells were further stained (red) with anti-Bip/GRP78 (B), anti-GM130 (E), or anti-EEA1 (H). Merged images are indicated to the right in each row (C, F, and I). Images were obtained by confocal microscopy. The EGFP-tagged Solo/Trio8 expression construct was transfected into 293 cells, and EGFP staining (green) was assessed. The 293 cells were further stained (red) for specific markers with anti-Rab5a (J), anti-Rab7 (K), or anti-Rab11 (L). Merged images are indicated, and colocalization is shown in yellow (blue arrowheads in J). Images were obtained with a charge-coupled device camera. Bars = 5  $\mu$ m.

Solo-AE, or EGFP-Solo-TM(-) expression construct (Fig. 3B, middle). Furthermore, the amount of EGFP-Solo did not differ between COS-7 cells transfected with WT or mutant Solo constructs (Fig. 3B, bottom).

**Solo/Trio8 localizes to early endosomes.** To address whether the potential C-terminal membrane-anchoring domain of Solo/Trio8 is required for membrane association, N-terminally FLAG-tagged Solo and Solo-TM(-) expression constructs (Fig. 3A) were transfected into COS-7 cells and the cell lysates

the respective positive and negative controls. (Middle) Total cell lysates probed for Rac1 demonstrate equal amounts of total Rac1 in all transfected cells. (Bottom) Expression of transfected proteins was evaluated by Western blotting with anti-GFP. The values on the left are molecular sizes in kilodaltons. (C) COS-7 cells were transfected with pCI-neo (mock), pCI-neo-FLAG-Solo, or pCI-neo-FLAG-Solo-TM(-). Soluble and membrane proteins were subjected to sodium dodecyl sulfate-polyacrylamide gel electrophoresis and immunoblotted with anti-FLAG, anti-1x-B (soluble-protein control), or anti-PDGFR $\alpha/\beta$  (membrane protein control). (D) Fluorescence microscopy of cells transfected with N- or C-terminally EGFP- or FLAG-tagged Solo or C-terminally truncated Solo-TM(-) expression constructs. Expression constructs encoding N-terminally EGFP-tagged Solo and Solo-TM(-) were transfected into COS-7 cells (a, b). Expression constructs of C-terminally FLAG-tagged Solo and Solo-TM(-) were transfected into COS-7 cells and stained with anti-FLAG (c, d). EGFP alone, C-terminally EGFP-tagged Solo, and Solo-TM(-) mutant expression constructs were transfected into NIH 3T3 cells (e to g). Bars = 10  $\mu$ m.

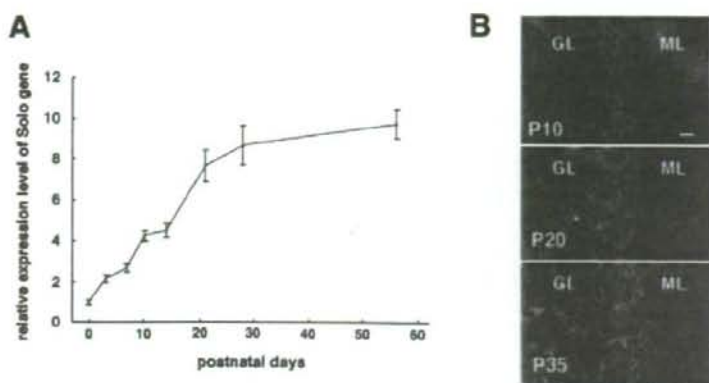


FIG. 5. Expression profile of Solo/Trio8 and the increase in the number of early endosomes during postnatal mouse cerebellar development. (A) SYBR green-based quantitative RT-PCR analysis of Solo/Trio8 transcript in WT mouse cerebellum during postnatal development. Expression levels are relative to P0 (P0 = 1.0). Each bar represents the mean  $\pm$  the standard error of the mean ( $n = 3$ ; three cerebella). (B) Immunohistochemistry of cerebellum sections during stages of postnatal maturation of Purkinje neurons (P10, P20, and P35). A section (20  $\mu$ m) was obtained from a C57BL/6J mouse brain. Sections were stained with anti-calbindin and coimmunostained with anti-EEA1. Merged images are shown in gray. Green lines indicate the location of each cell body of calbindin-positive Purkinje neurons. Bright, dot-like signals indicate EEA1-positive early endosomes. GL, granule cell layer; ML, molecular cell layer. Bar = 20  $\mu$ m.

were analyzed by Western blotting. N-terminally FLAG-tagged Solo was a single band of  $\sim$ 220 kDa that localized to both soluble and membrane fractions (Fig. 3C). Nearly all of the N-terminally FLAG-tagged Solo-TM(-) was found in the soluble fraction (Fig. 3C), indicating that the C-terminal domain is essential for membrane anchoring. The internal control proteins I $\kappa$ B (soluble) and PDGF receptor  $\alpha/\beta$  (membrane associated) were detected in the appropriate fractions (Fig. 3C). The subcellular localization of Solo was confirmed by immunofluorescence microscopy of N- or C-terminally EGFP- or FLAG-tagged Solo constructs. The N-terminally tagged construct displayed a pattern consistent with localization to the cytoplasm and to small vesicles in COS-7 cells (Fig. 3D, a; Fig. 4A, D, and G), 293 cells (Fig. 4J to L), and primary cultured neurons (see Fig. 7D). The C-terminally tagged protein yielded similar results (Fig. 3D, c, COS-7; Fig. 3D, f, NIH 3T3). N-terminally and C-terminally EGFP- or FLAG-tagged Solo-TM(-) displayed uniform cytoplasmic localization (Fig. 3D, b, d, and g). These results indicated that the putative C-terminal membrane-anchoring domain is essential for vesicular localization. Although various N-terminally truncated Solo mutant constructs generated by serial deletion of N-terminal domains, including the sec14-like and spectrin-repeat domains, also failed to distribute to vesicles, Western blotting revealed that these mutant proteins were not stable in COS-7 cells (data not shown).

Subcellular localization of Solo/Trio8 was then analyzed with organelle-specific markers. Antibodies against Bip/GRP78, GM130, and EEA1 specifically label the endoplasmic reticulum (22, 31), Golgi (1), and early endosomes (5, 9), respectively (Fig. 4B, E, and H). Of these markers, only the signal for the early-endosome marker EEA1 partially overlapped the EGFP-Solo signal (Fig. 4A to I), suggesting that Solo/Trio8 localizes to early endosomes. To confirm the localization with other endosomal markers and another cell type, we stained EGFP-Solo-expressing 293 cells with specific anti-

bodies to Rab5 for early endosomes (28), Rab7 for late endosomes (11), and Rab11 for recycling endosomes (40). EGFP-Solo staining partially overlapped Rab5-positive vesicles (Fig. 4J) but not Rab7- or Rab11-positive vesicles (Fig. 4K and L). These data indicated that Solo/Trio8 localizes to early endosomes. However, at this level of resolution, we could not rule out the possibility that the observed colocalization of Solo with EEA1 and Rab5 arose from coincidental overlap due to the high-density punctate staining resulting from overexpression of these proteins.

We could not define which subclass of early endosomes expressed Solo/Trio8 because specific markers for such a classification are not available.

**Solo/Trio8 gene expression correlates with early-endosome maturation levels in postnatal Purkinje neuronal cells.** We analyzed the temporal pattern of the Solo/Trio8 gene expression level during Purkinje neuron maturation after birth (Fig. 5A). Analysis of mRNA samples prepared from P0 to P56 cerebella showed that the gene for Solo/Trio8 was expressed after birth, markedly increased during the first 4 weeks of life, and achieved maximal levels during adulthood. To investigate the development of early endosomes in Purkinje neurons, we stained cerebellar brain sections with antibodies against EEA1 and calbindin D28k (Purkinje neuron marker) (34). The number of large EEA1-positive early endosomes increased in Purkinje neurons during the postnatal maturation stage after P20 (Fig. 5B), indicating a correlation between expression levels of Solo/Trio8 and early-endosome development in D28k-positive Purkinje neurons.

**Solo/Trio8 modulates early-endosome dynamics via its GEF1 activity and C-terminal membrane-anchoring domain.** We assessed the effect of Solo overexpression on EEA1-positive early endosomes in COS-7 cells. The average number of EEA1-positive early endosomes increased in EGFP-Solo-expressing cells (1.84-fold  $\pm$  0.217-fold versus EGFP alone;  $P < 0.001$ ,  $n = 40$ ; Fig. 6A and B). We next addressed whether

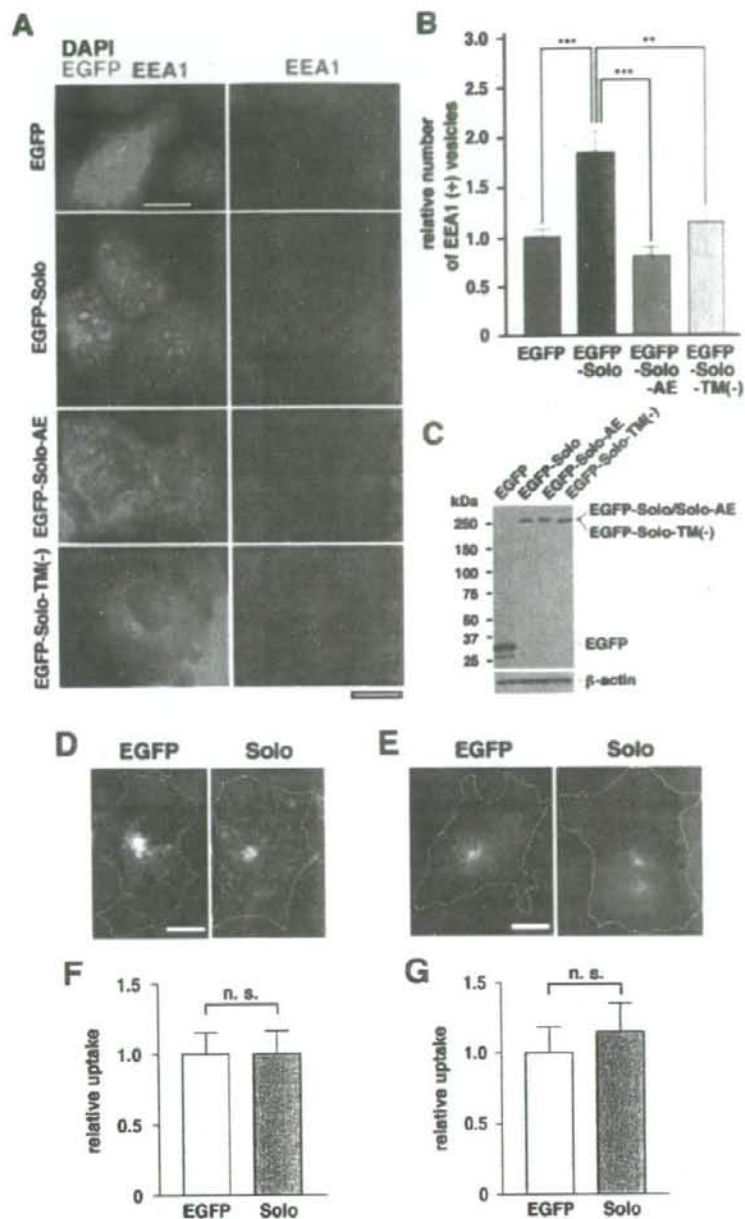


FIG. 6. Solo/Trio8 modulates early-endosome dynamics. (A) Expression constructs of the control EGFP, EGFP-Solo, EGFP-Solo-AE (GEF1 inactive form), and EGFP-Solo-TM(-) were transfected into COS-7 cells (EGFP signal is indicated in green). At 8 h posttransfection, cells were stained with anti-EEA1 (red) and DAPI (blue). Merged tricolor images are shown to the left. For ease of visualization, two-color images (minus the green EGFP signal) are shown to the right. Dotted lines indicate cellular edges. Images were obtained with a cooled charge-coupled device camera. Bars = 10  $\mu$ m. (B) Quantification of EEA1-positive vesicles (early endosomes; survey square,  $>0.04 \mu\text{m}^2$ ) in COS-7 cells transfected with EGFP-expressing cells (negative control; EGFP = 1.0). Each bar represents the mean  $\pm$  the standard error of the mean ( $n = 40$  cells for each construct). \*\*,  $P < 0.01$ ; \*\*\*,  $P < 0.001$ . (C) Protein expression levels of EGFP (negative control), EGFP-Solo, EGFP-Solo-AE, and EGFP-Solo-TM(-) constructs were analyzed by Western blotting (8  $\mu$ g protein per lane) with anti-Living Colors A.v. for EGFP detection.  $\beta$ -Actin expression was monitored as an internal control. (D to G) Effect of Solo/Trio8 on endocytosis. COS-7 cells expressing EGFP or EGFP-Solo were



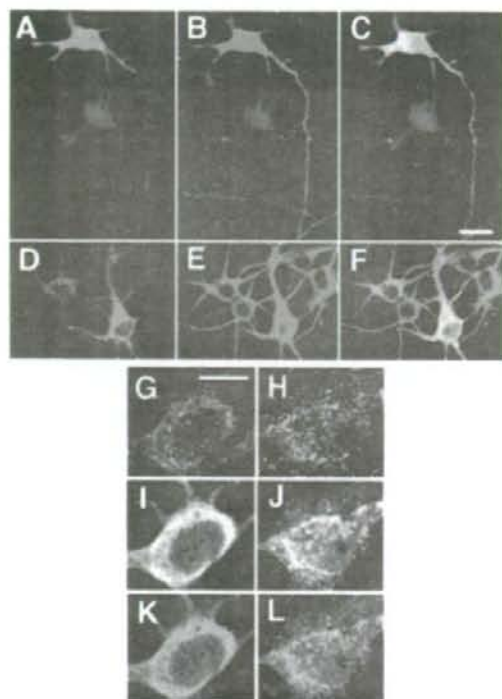


FIG. 7. Subcellular localization of Solo/Trio8 in cultured cortical neurons transfected with the EGFP-tagged Solo expression construct. EGFP signal (green) was observed in axons (A) and dendrites (D). These same cells were stained with anti-Tau1 (B) and anti-Map2 (E). Merged images are indicated to the right in each row (C and F). Images were obtained by confocal microscopy. Bar in panel C = 20  $\mu$ m (same scale for panels A to F). (G to L) Cultured cortical neurons transfected with the EGFP (I) or EGFP-tagged Solo (J) expression construct. These same cells were stained with anti-Rab5a (G and H). Merged images are indicated in the lower panels (K, EGFP and Rab5a; L, EGFP-Solo and Rab5a). Bar in panel G = 10  $\mu$ m (same scale for panels G to L).

GEF1 activity is required to induce the increase in EEA1-positive early endosomes with the double mutant Solo-AE (Fig. 3A), which lacks guanine nucleotide exchange activity for Rac1 (Fig. 3B). The endosome-inducing activity of this mutant was compared with that of EGFP-Solo. As expected, expression of EGFP-Solo-AE did not increase the number of EEA1-positive early endosomes (Fig. 6A and B). However, the lack of GEF1 activity altered the early-endosomal location of Solo/Trio8 (Fig. 6A). On the other hand, the distribution pattern of Solo-AE resembled that expected for lysosomal membranes,

suggesting that the GEF1 activity is involved in selective transfer of Solo/Trio8 from early endosomes to late endosomes-lysosomes. Given that the Solo membrane-anchoring domain is required for membrane localization (Fig. 3C and D), we further addressed whether this domain is required to induce an increase in the number of EEA1-positive endosomes. The truncated mutant Solo-TM(-) did not increase the number of EEA1-positive endosomes (Fig. 6A and B). On the other hand, EGFP-Solo did not significantly affect the size of individual EEA1-positive early endosomes relative to EGFP-Solo mutants (data not shown). Western blotting and immunofluorescence microscopy of EGFP-derived signals in COS-7 cells confirmed that the expression levels and integrity of EGFP-Solo-AE and EGFP-Solo-TM(-) were similar to those of EGFP-Solo (Fig. 6A and C). To probe the mechanism of the Solo/Trio8-induced increase in early endosomes, we investigated the effect of Solo/Trio8 expression on endocytosis in COS-7 cells. The uptake of Alexa Fluor 594-labeled human transferrin and Sulforhodamine 101 did not change in EGFP-Solo-transfected COS-7 cells compared with control EGFP-transfected cells (Fig. 6D to G), suggesting that Solo/Trio8 modulates early-to-late or early-to-recycling endosome transfer rather than endocytosis.

**Solo/Trio8 localizes in axons and somatodendrites in primary cultured neurons.** The gene for Solo/Trio8 is expressed in Purkinje neurons (Fig. 2B). Mature neurons have two polarized subcellular compartments, namely, axons and somatodendrites. Epithelial cells, including neurons, have polarized endosomes, that is, apical (axonal) endosomes and basolateral (somatodendrite) endosomes (2). To assess whether Solo/Trio8 localizes to early endosomes in a cell polarity-dependent manner in neuronal cells, we analyzed the EGFP-Solo distribution in primary cultured neurons. EGFP-Solo localized to small, Rab5-positive vesicles in soma (Fig. 7G to L), indicating localization to early endosomes. Moreover, EGFP-Solo was detected both in Map2-positive dendrites and in Tau1-positive axons (Fig. 7A to F). These results indicated that Solo localizes to both axons and somatodendrites in a cell polarity-independent manner.

**Solo/Trio8 promotes neurite elongation in primary cultured neurons.** Since endosomal membrane trafficking in neurons is involved in the regulation of neurite morphology (16, 19, 33), we analyzed the effects of Solo/Trio8 on neurite morphology in primary cultured cortical neurons. The total neurite length (axon and dendrite length) of the cortical neurons transfected with the EGFP-Solo expression construct significantly increased (about twofold) compared with cells transfected with the negative control EGFP construct (EGFP versus EGFP-Solo =  $718.1 \pm 66.8 \mu$ m versus  $1,321.0 \pm 111.4 \mu$ m;  $n = 74$  and  $97$  neurons, respectively;  $P < 0.01$ ; Fig. 8A and D). The EGFP-Solo expression construct also significantly increased (about twofold) the average maximal axon length in the primary cul-

incubated with Alexa 594-conjugated transferrin (25  $\mu$ g/ml; D) or Sulforhodamine 101 (25  $\mu$ g/ml; E) for 15 min and then fixed. Internalized transferrin or sulforhodamine (F and G) after 15 min of uptake was quantified by measuring the fluorescence intensity per cell as detected in panels D and E. The uptake of fluorescence for each construct is presented relative to that for EGFP-expressing cells (negative control; EGFP = 1.0). Each bar represents the mean  $\pm$  the standard error of the mean ( $n > 10$  cells for each construct). The differences in uptake between EGFP- and EGFP-Solo-expressing COS-7 cells were not significant (n.s.). Scale bars = 10  $\mu$ m.

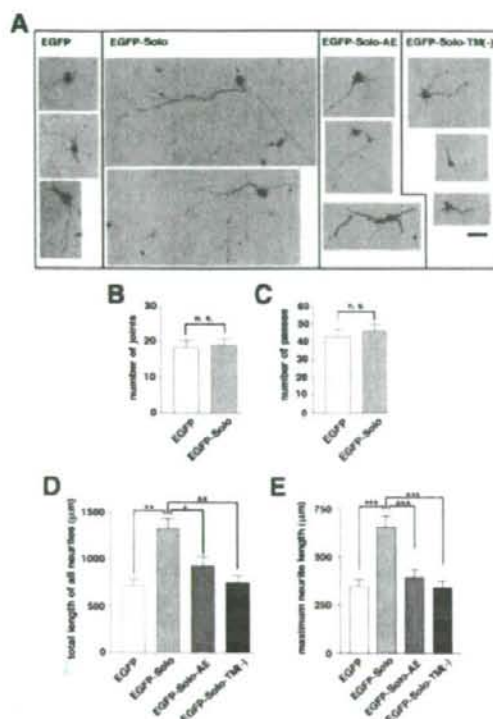


FIG. 8. Effects of Solo/Trio8 on neurite elongation in cultured cortical neurons. (A) Morphology of EGFP-Solo- or EGFP-Solo mutant-expressing neurons with anti-DsRed staining. Representative examples of fluorescence images (DsRed-derived signal; dark signals) of neurons transfected with control EGFP, EGFP-Solo, EGFP-Solo-AE, or EGFP-Solo-TM(-) constructs together with DsRed at 6 days in vitro are shown. To visualize the transfected neurons and their morphology, neurons were fixed and coimmunostained with anti-DsRed and anti-EGFP. Scale bar = 100  $\mu$ m. (B and C) Quantification of the effects of EGFP and EGFP-Solo expression on the number of joints (branch points) (B) and passes (branch number) (C) per neuron (EGFP,  $n = 74$ ; EGFP-Solo,  $n = 97$ ). n.s., no significant difference. (D and E) Quantification of the effects of EGFP, EGFP-Solo, EGFP-Solo-AE, and EGFP-Solo-TM(-) expression on neurite length (total neurite length per neuron, dendrite length plus axon length) (D) and average maximal neurite length (axon length per neuron) (E) [EGFP,  $n = 74$ ; EGFP-Solo,  $n = 97$ ; EGFP-Solo-AE,  $n = 60$ ; EGFP-Solo-TM(-),  $n = 91$ ]. Each bar represents the mean  $\pm$  the standard error of the mean. \*,  $P < 0.05$ ; \*\*,  $P < 0.01$ ; \*\*\*,  $P < 0.001$ .

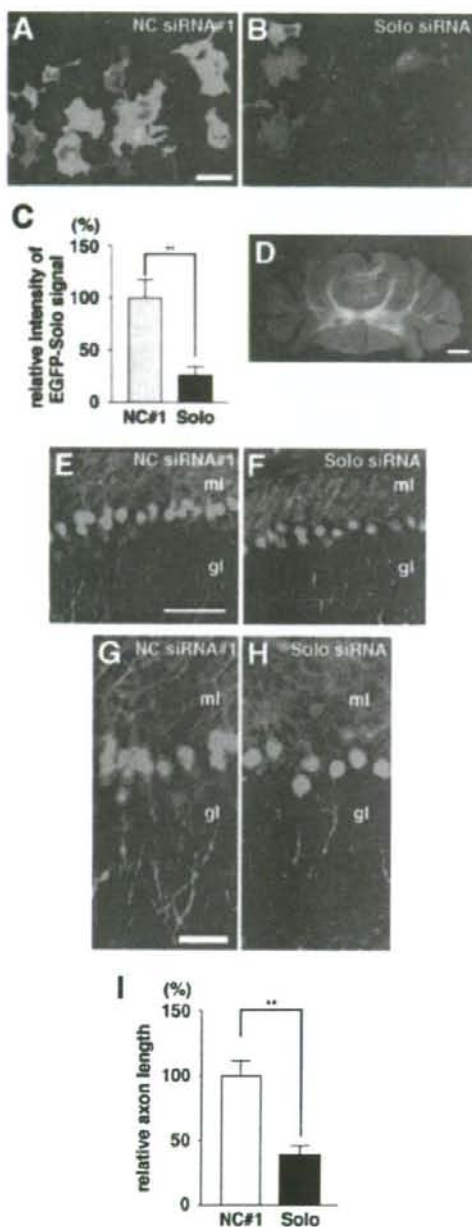
tured neurons (EGFP versus EGFP-Solo =  $347.3 \pm 35.64 \mu$ m versus  $650.9 \pm 60.94 \mu$ m;  $n = 74$  and  $97$  neurons, respectively;  $P < 0.001$ ; Fig. 8E). Mutant Solo expression constructs EGFP-Solo-AE and EGFP-Solo-TM(-) failed to induce either total neurite length or maximal elongation (Fig. 8A, D, and E). The number of joints (branch points) and passes (branches) did not change significantly upon EGFP-Solo expression (Fig. 8B and C). We were unable to quantify the total number of early endosomes per neuron because the size and complexity of neurons relative to COS-7 cells (Fig. 6) precluded the detection of all early endosomes with sufficient resolution in a single

image. However, EGFP-Solo was distributed in a vesicle-like pattern (similar to that in COS-7 cells) in axons and dendrites of neurons (Fig. 7 and data not shown), and this pattern was altered upon expression of Solo-AE or Solo-TM(-) (data not shown), as observed in COS-7 cells (Fig. 6A).

Solo/Trio8 siRNA affects calbindin D28k-positive neurite length in the granule cell layer of the cerebellum. We attempted to knock down expression of the gene for Solo/Trio8 by RNA interference. To find an RNA sequence that would be effective, we prepared seven siRNAs with different Solo/Trio8-specific target recognition sequences that lacked homology to other sequences in the mouse genome. We then transfected each siRNA together with the EGFP-Solo expression construct into COS-7 cells. Transfection of the siRNA (region, bp 5483 to 5505) with a target sequence in the potential membrane-anchoring domain of Solo significantly reduced the level of Solo protein by  $\sim 25\%$  (Fig. 9B and C) compared with that of COS-7 cells transfected with negative control scrambled siRNA no. 1 (Fig. 9A and C), negative control siRNA no. 2 (purchased from Ambion), or no siRNA (data not shown). The Solo/Trio8-specific siRNA did not affect the level of EGFP in cells transfected with the EGFP expression construct compared with negative control siRNA (data not shown). To investigate the role of Solo/Trio8 in neurite morphology, we transfected the Solo/Trio8-specific siRNA or negative control scrambled siRNAs into cells of organotypic brain slices (44) by a liposome-based in vivo siRNA-transfer method (51) that we had previously established. We prepared coronally sliced P11 cerebellar slices and cut them into left and right halves (Fig. 9D). One of the halves was transfected with Solo/Trio8-specific siRNA, and the other half was transfected with negative control siRNA. We confirmed efficient incorporation of transfected Cy3-labeled control siRNA no. 1 into cells in the cerebellar slice by confocal laser scanning microscopy (data not shown). We fixed the slices 2 days after transfection and stained them with anti-calbindin D28k to specifically visualize the morphology of Purkinje neurons. The lengths of calbindin D28k-positive neurites (axons of Purkinje neurons) in the granule cell layer of slices transfected with Solo/Trio8 siRNA were significantly shorter (39.2%;  $n = 4$ ;  $P = 0.0039$ , Student's  $t$  test) than those of slices transfected with negative control siRNA no. 1 (Fig. 9E to I), suggesting that Solo/Trio8 is essential for neurite elongation or maintenance of Purkinje axon length. The neurite morphology of neurons transfected with negative control siRNA no. 1, siRNA no. 2, or EGFP siRNA (purchased from Ambion) was not changed compared with that of untransfected Purkinje neurons (data not shown).

## DISCUSSION

A number of early-endosome-specific proteins have been identified to date. Among them, EEA1, a specific effector of Rab5, binds to early-endosomal membranes (5, 45). This localization of EEA1 is mediated via its FYVE domain that interacts with phosphatidylinositol 3-phosphate, whose intracellular distribution is restricted primarily to early endosomes (21). In the present study, DNA microarray analysis of *pcd* mice led us to identify a mouse Trio splice variant, Solo/Trio8, which localizes to early endosomes. Although Solo/Trio8 is likely embedded in the endosomal membrane (Fig. 3, 4, 6, and



**FIG. 9.** Effects of Solo/Trio8 siRNA on Purkinje neurons. COS-7 cells were cotransfected with vectors encoding either EGFP-Solo and control scrambled siRNA (A, negative control [NC] siRNA no. 1) or EGFP-Solo and Solo/Trio8 siRNA (B, Solo siRNA) and then stained with anti-GFP (green) and DAPI (blue). (C) Effect of siRNA on EGFP-Solo expression quantified by measuring the fluorescence intensity per cell as detected in panels A and B. The effect of Solo siRNA on EGFP-Solo suppression is presented relative to that of negative control siRNA no. 1 (100%). Each bar represents the mean  $\pm$  the standard error of the mean ( $n > 10$  cells). Significant differences are

7), it does not contain a canonical FYVE-like motif. It is not clear which domain actively recruits Solo/Trio8 to early endosomes; however, an N-terminal region may be required for the recruitment since this region contains a *sec14*-like domain and spectrin-like repeats. Yeast Sec14 is a phosphatidylinositol transfer protein that catalyzes the exchange of phosphatidylinositol for phosphatidylcholine in membranes (43), suggesting that the *sec14*-like domain of Solo/Trio8 may function to link it to phosphatidylinositol 3-phosphate in early endosomes. The spectrin-like repeats constitute interaction sites for cytoskeletal and signal transduction proteins (8) and may facilitate the association of Solo/Trio8 (directly or indirectly) with early-endosome membranes. Cooperative interactions between the N- and C-terminal domains are likely to be important for targeting Solo to the early endosome and thus may represent a novel mechanism for protein localization to this organelle.

Solo/Trio8 mRNA expression was restricted to Purkinje neurons in the cerebellum and markedly increased during the maturation stage of these neurons after birth (Fig. 5A). EEA1-positive early-endosome signals also markedly increased in Purkinje neurons during this stage (Fig. 5B). We demonstrated that overexpression of Solo/Trio8 augmented the number of EEA1-positive early-endosomal vesicles in COS-7 cells, and the abrogation of Solo GEF1 activity attenuated this increase and disrupted the cellular distribution of early endosomes (Fig. 6). Taken together, these results suggest that Solo/Trio8 promotes postnatal maturation of the early-endosome pool in Purkinje neurons. Our data also suggest that Solo/Trio8 GEF1 activity is essential for the localization of this protein to early endosomes, and it may affect the maturation of the early-endosome pool directly via some small GTPases. The Trio GEF1 domain activates both Rac1 (Fig. 3B) and RhoG (3), and therefore Solo/Trio8 GEF1 may also activate downstream early-endosomal Rac1- or RhoG-type small GTPases. More than 150 small GTPases have been identified in the human genome, and the Rac1- and RhoG-type subfamily includes Rac1 to -3, RhoG, CDC42h, CDC42, TC10, and TCL (15). Among these, Rac1 and TC10 are present in endosomes (26, 27) but it is not known if either protein is a direct target for Solo/Trio8 GEF1 in early endosomes. Solo/Trio8 may activate multiple Rac1/RhoG-type small GTPases, each of which may

indicated by double asterisks ( $P < 0.01$ ; *t* test). Scale bar = 50  $\mu$ m. (D) Overview of a coronally sliced cerebellum. Scale bar = 1 mm. Cerebellar slices derived from P11 were cut into left and right halves (at the red dotted line). One of the halves was transfected with Solo/Trio8-specific siRNA (F and H; Solo siRNA), and the another half was transfected with negative control siRNA no. 1 (E and G) at 1 day in vitro and then cultured for 2 days. Slices were stained with anti-calbindin D28k (green), showing the morphology of Purkinje cells. Panels G and H are high-magnification images of panels E and F, respectively. gl, granule cell layer; ml, molecular cell layer. The scale bar in panel E is 100  $\mu$ m (E and F), and that in panel G is 50  $\mu$ m (G and H). (I) Quantitative representation of the effect of Solo/Trio8 siRNA on the axon length of Purkinje neurons in the granule cell layer. The relative axon length for Solo siRNA is presented relative to that for negative control siRNA no. 1 (100%). Each bar represents the mean  $\pm$  the standard error of the mean ( $n = 4$  slices). Significant differences are indicated by double asterisks ( $P < 0.01$ ; *t* test).

have a discrete function in early endosomes. Cellular Rac1 (26) had a distribution pattern distinct from that of Solo/Trio8, and Rac1 activation (Fig. 3) did not correlate with the increase in early endosomes induced by WT or mutant Solo/Trio8 (Fig. 6). Thus, Rac1 is unlikely to be the direct downstream target of Solo/Trio8. Identification of *in vivo* downstream targets for Solo/Trio8 may enhance our understanding of how Rho family GTPases regulate endosomal vesicle trafficking.

EGFP-Solo proteins were distributed in Tau1-positive axons, Map2-positive dendrites were distributed in cortical neurons (Fig. 7), and transfection of the EGFP-Solo construct induced both dendrite and axon elongation in these neurons (Fig. 8). These data indicate that Solo/Trio8 functions in a cell polarity-independent manner to regulate neuronal morphology. Furthermore, GEF1 activity and the C-terminal membrane-anchoring domain of Solo/Trio8 were essential for induction of not only neurite elongation but also of an increase in the number of early endosomes (Fig. 6 and 8). These equivalent domain requirements indicate that both biological activities are exhibited upon activation of early-endosome-associated Rho family GTPases, suggesting that Solo/Trio8 functions as an early-endosome-associated GEF to control cell polarity-independent neurite morphogenesis.

To date, two Trio family members, Trio and Kalirin, have been identified in mammals (3). The domain structure of Kalirin is nearly identical to that of Trio, and its expression is specific to the central nervous system (3). In addition, several short isoforms of Kalirin have been identified (18). Full-length Kalirin localizes to neuronal soma, where it displays a cytoplasmic protein-like diffuse immunostaining pattern. Interestingly, a Kalirin splice variant, Duo/Kalirin-7, lacking the C-terminal GEF2 and kinase domains (that is, a structure similar to that of Solo/Trio8) localizes to small punctate structures at neuronal processes and dendritic spines (18, 38). Duo/Kalirin-7 is involved in signal transduction during dendritic spine morphogenesis mediated by activation of the ephrinB receptor (37). We thus postulate that some of the cell surface receptors or adhesion molecules controlling neurite morphology are involved in Solo/Trio8-induced neurite elongation via the regulation of early-endosome dynamics.

Upstream effectors of endosome-specific Rab family small GTPases that localize to early endosomes have previously been characterized (39, 46). However, the activation mechanism of Rho family small GTPases that function in early endosomes is not well understood. Here, we identified Solo/Trio8 as a candidate upstream effector of Rho family GTPases that localize to early endosomes. The subcellular localization of Solo/Trio8 is mediated through a C-terminal membrane-anchoring domain and its GEF1 activity (Fig. 6A, EGFP-Solo-AE), and it is plausible that its endosomal localization may directly activate Rac1/RhoG-type small GTPases that sequentially modulate the dynamics of early endosomes. Our results show that Solo/Trio8 gene expression significantly increases during the postnatal maturation stage of Purkinje neurons in the cerebellum (Fig. 5). We also demonstrate that a Solo/Trio8-specific siRNA induces loss of calbindin D28k-positive neurite morphology in cultured cerebellar slices (Fig. 9). These data suggest that changes in early-endosome dynamics, as modulated by Solo, control neurite morphogenesis and/or maintenance of Purkinje neurons *in vivo*.

#### ACKNOWLEDGMENTS

This work was supported by Grants-in-Aid for Scientific Research from the Ministry of Health, Labor and Welfare of Japan; Grants-in-Aid for Scientific Research from the Ministry of Education, Culture, Sports, Science and Technology of Japan; a grant from Pharmaceuticals and Medical Devices Agency; and a grant from the Japan Science and Technology Agency.

#### REFERENCES

- Aoki, S., Q. Su, H. Li, K. Nishikawa, K. Ayukawa, Y. Hara, K. Namikawa, S. Kiryu-Seo, H. Kiyama, and K. Wada. 2002. Identification of an axotomy-induced glycosylated protein, ALGP1, possibly involved in cell death triggered by endoplasmic reticulum-Golgi stress. *J. Neurosci.* **22**:10751-10760.
- Apodaca, G. 2001. Endocytic traffic in polarized epithelial cells: role of the actin and microtubule cytoskeleton. *Traffic* **2**:149-159.
- Bateman, J., and D. Van Vactor. 2001. The Trio family of guanine-nucleotide-exchange factors: regulators of axon guidance. *J. Cell Sci.* **114**:1973-1980.
- Benard, V., and G. M. Bokoch. 2002. Assay of Cdc42, Rac, and Rho GTPase activation by affinity methods. *Methods Enzymol.* **345**:349-359.
- Christoforidis, S., H. M. McBride, R. D. Burgoyne, and M. Zerial. 1999. The Rab5 effector EEA1 is a core component of endosome docking. *Nature* **397**:621-625.
- Debant, A., C. Serra-Pages, K. Seipel, S. O'Brien, M. Tang, S. H. Park, and M. Streuli. 1996. The multidomain protein Trio binds the LAR transmembrane tyrosine phosphatase, contains a protein kinase domain, and has separate rac-specific and rho-specific guanine nucleotide exchange factor domains. *Proc. Natl. Acad. Sci. USA* **93**:5466-5471.
- Delcroix, J. D., J. S. Valletta, C. Wu, S. J. Hunt, A. S. Kowal, and W. C. Mobley. 2003. NGF signaling in sensory neurons: evidence that early endosomes carry NGF retrograde signals. *Neuron* **39**:69-84.
- Djinovic-Carugo, K., M. Gautel, J. Ylanne, and P. Young. 2002. The spectrin repeat: a structural platform for cytoskeletal protein assemblies. *FEBS Lett.* **513**:119-123.
- Dumas, J. J., E. Merithew, E. Sodharshan, D. Rajamani, S. Hayes, D. Lawe, S. Corvera, and D. G. Lambright. 2001. Multivalent endosome targeting by homodimeric EEA1. *Mol. Cell* **8**:947-958.
- Estrach, S., S. Schmidt, S. Diriong, A. Penna, A. Blangy, P. Fort, and A. Debant. 2002. The human Rho-GEF trio and its target GTPase RhoG are involved in the NGF pathway, leading to neurite outgrowth. *Curr. Biol.* **12**:307-312.
- Feng, Y., B. Press, and A. Wandinger-Ness. 1995. Rab 7: an important regulator of late endocytic membrane traffic. *J. Cell Biol.* **131**:1435-1452.
- Fernandez-Gonzalez, A., A. R. La Spada, J. Treadaway, J. C. Higdon, B. S. Harris, R. L. Sidman, J. I. Morqun, and J. Zuo. 2002. Purkinje cell degeneration (pcd) phenotypes caused by mutations in the axotomy-induced gene, *Nna1*. *Science* **295**:1904-1906.
- Gasman, S., Y. Kalaidzidis, and M. Zerial. 2003. RhoD regulates endosome dynamics through Diaphanous-related Formin and Src tyrosine kinase. *Nat. Cell Biol.* **5**:195-204.
- Gomez, G. A., and J. L. Daniotti. 2005. H-Ras dynamically interacts with recycling endosomes in CHO-K1 cells: involvement of Rab5 and Rab11 in the trafficking of H-Ras to this pericentriolar endocytic compartment. *J. Biol. Chem.* **280**:34997-35010.
- Heo, W. D., and T. Meyer. 2003. Switch-of-function mutants based on morphology classification of Ras superfamily small GTPases. *Cell* **113**:315-328.
- Huang, E. J., H. Li, A. A. Tang, A. K. Wiggins, R. L. Neve, W. Zhong, L. Y. Jan, and Y. N. Jan. 2005. Targeted deletion of numb and numlike in sensory neurons reveals their essential functions in axon arborization. *Genes Dev.* **19**:138-151.
- Jarousse, N., and R. B. Kelly. 2001. Endocytic mechanisms in synapses. *Curr. Opin. Cell Biol.* **13**:461-469.
- Johnson, R. C., P. Penzes, B. A. Eipper, and R. E. Mains. 2000. Isoforms of kalirin, a neuronal Dbl family member, generated through use of different 5' and 3'-ends along with an internal translational initiation site. *J. Biol. Chem.* **275**:19324-19333.
- Kimura, K., A. Mizoguchi, and C. Ide. 2003. Regulation of growth cone extension by SNARE proteins. *J. Histochem. Cytochem.* **51**:429-433.
- Kroschewski, R., A. Hall, and I. Mellman. 1999. Cdc42 controls secretory and endocytic transport to the basolateral plasma membrane of MDCK cells. *Nat. Cell Biol.* **1**:8-13.
- Kutateladze, T., and M. Overduin. 2001. Structural mechanism of endosome docking by the FYVE domain. *Science* **291**:1793-1796.
- Linnik, K. M., and H. Hersevoort. 1998. Multiple molecular chaperones interact with apolipoprotein B during its maturation. The network of endoplasmic reticulum-resident chaperones (ERp72, GRP94, calreticulin, and BiP) interacts with apolipoprotein B regardless of its lipidation state. *J. Biol. Chem.* **273**:21368-21373.
- Liu, X., H. Wang, M. Eberstadt, A. Schnuchel, E. T. Olejniczak, R. P. Meadows, J. M. Schkeryantz, D. A. Janowick, J. E. Harlan, E. A. Harris, D. E. Staunton, and S. W. Fesik. 1998. NMR structure and mutagenesis of